Final Technical Report (FTR)

Cover Page

a. *Federal Agency*	Department of Energy Solar Energy Technologies Office	
b. *Award Number*	DE-EE0010249	
c. *Project Title*	In-situ hydrogen microstructural characterization of Si heterojunction passivation: Addressing V_{OC} degradation and mitigation pathways	
d. *Recipient Organization*	University of Delaware	
e. *Project Period*	*Start:* 10/01/2023	*End:* 3/31/2024
f. *Principal Investigator (PI)*	Name: Ujjwal Das Title: Senior Scientist Email address: ukdas@udel.edu Phone number: 302-831-3523	
g. *Business Contact (BC)*	Name: Susan Tompkins Title: Assistant Director, Contracts & Grants Email address: sdt@udel.edu Phone number: 302-831-8002	
h. *Certifying Official (if different from the PI or BC)*	Name Title Email address Phone number	

Signature of Certifying Official *Date: 7/29/2024*

By signing this report, I certify to the best of my knowledge and belief that the report is true, complete, and accurate. I am aware that any false, fictitious, or fraudulent information, misrepresentations, half-truths, or the omission of any material fact, may subject me to criminal, civil or administrative penalties for fraud, false statements, false claims or otherwise. (U.S. Code Title 18, Section 1001, Section 287 and Title 31, Sections 3729-3730). I further understand and agree that the information contained in this report are material to Federal agency's funding decisions and I have any ongoing responsibility to promptly update the report within the time frames stated in the terms and conditions of the above referenced Award, to ensure that my responses remain accurate and complete.

1. Acknowledgement: "This material is based upon work supported by the U.S. Department of Energy's Office of Energy Efficiency and Renewable Energy (EERE) Solar Energy Technologies Office (SETO) under the Small Innovative Projects in Solar 2022 Award Number [DE-EE0010249]."

any legal liability or responsibility for the accuracy, completeness, or usefulness of any information, apparatus, product, or process disclosed, or represents that its use would not infringe privately owned rights. Reference herein to any specific commercial product, process, or service by trade name, trademark, manufacturer, or otherwise does not necessarily constitute or imply its endorsement, recommendation, or favoring by the United States Government or any agency thereof. The views and opinions of authors expressed herein do not necessarily state or reflect those of the United States Government or any agency thereof."

3. Executive Summary:

Si heterojunction (SHJ) solar cells have demonstrated record efficiency >27%, approaching the theoretical limit of ≈ 29%, primarily due to best surface/interface defect passivation provided by deposited thin layers of hydrogenated amorphous silicon (a-Si:H). Such excellent surface/interface passivation reduces recombination loss and result in >100 mV improvement of cell open circuit voltage (V_{OC}) to ≈ 750 mV, thus the cell efficiency. However, fielded SHJ modules exhibit loss of V_{OC} and hence efficiency over time in years, presumably due to degradation related to a-Si:H layers. This adversely affects the technology's market acceptance, and levelized cost of energy (LCOE). It is hypothesized that the origin of a-Si:H degradation is somehow related to the presence of weak Si–Si bonds and hydrogen in a-Si:H films. The objective of this project is to test this hypothesis by directly measuring chemical and structural changes occurring within SHJ component layers and solar cells. This is achieved by developing an innovative in-situ Fourier transform infrared (FTIR) spectrometry apparatus to monitor hydrogen microstructural changes occurring within amorphous silicon and decipher hydrogen evolution kinetics over time when samples are exposed to heat and/or light stress. These in-situ measured hydrogen microstructural changes are correlated to the changes in effective minority carrier lifetime (τ_{eff}), implied V_{OC} (iV_{OC}), surface recombination velocity (S), and cell V_{OC}. These mechanistic understandings will provide critical guidance to mitigate the V_{OC}-driven degradation of SHJ solar cell performance.

Passivation optimization and degradation analysis of individual SHJ component structures were achieved through systematic deposition of three symmetric structures and the completed SHJ solar cell structure shown in Fig.1. The three symmetric structures used were intrinsic a-Si:H [(i)a-Si:H] layers in a bilayer structure [Fig.1(a)], intrinsic and p-type doped stacked layers [(i-p)a-Si:H] representing the front heterojunction [Fig.1(b)] in the SHJ cell, and intrinsic and n-typed doped stacked layers [(i-n)a-Si:H] representing the back-side back surface field (BSF) [Fig.1(c)] in the SHJ cell. State-of-the-art passivation qualities are demonstrated by a champion iV_{OC} of 740 mV for the (i)a-Si:H layers, and the (i-n)a-Si:H symmetric structure. A 725 mV iV_{OC} is observed for the (i-p)a-Si:H symmetric structure.

These symmetric passivated SHJ component structures were subsequently subjected to different accelerated lifetime (ALT) stressors to identify which conditions contribute the most to iV_{OC} degradation. Degradation of the thin (10 nm) (i)a-Si:H passivation layers without any additional overlying layers is minimal; complexity of this study arises due to unavoidable surface oxidation of (i)a-Si:H layer during most of the stress application, which is likely irrelevant for a full SHJ cell configuration with overlying protective layers.

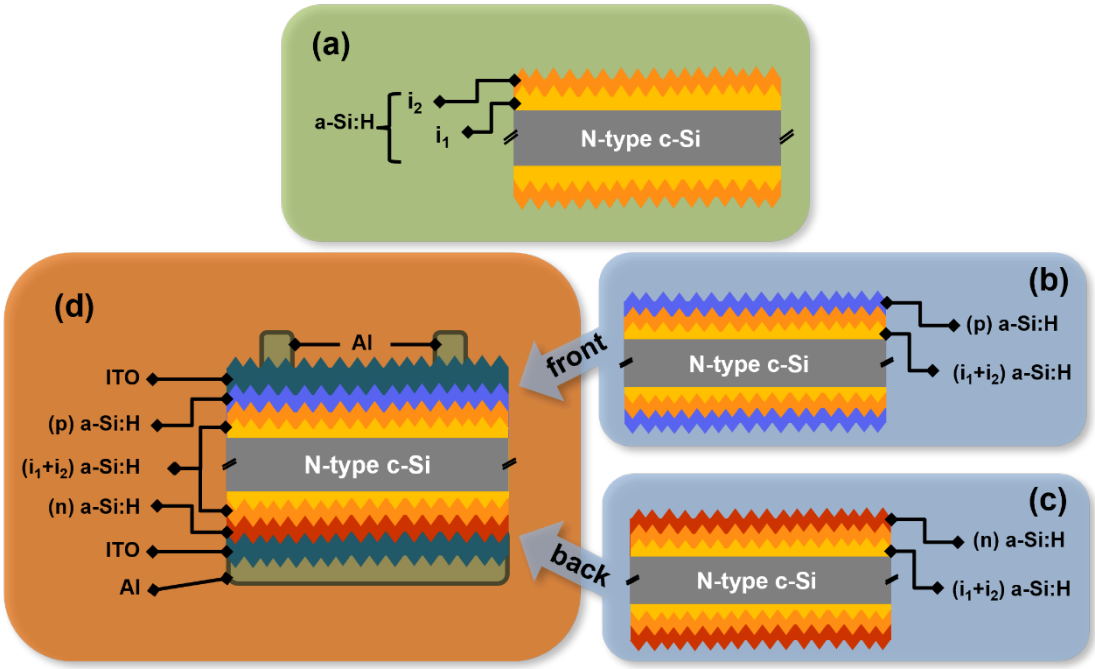

Fig. 1: Schematics of different SHJ passivation structures using (a) symmetric (i)a-Si:H stack layer, (b) symmetric (i-p)a-Si:H, (c) symmetric (i-n)a-Si:H, and (d) completed SHJ solar cell studied in this project.

The iV_{OC} degradation of symmetric structures is found to occur primarily at the (i-p)a-Si:H passivation stack under dark heat stress with associated hydrogen loss from the (p)a-Si:H layer. An activation energy for increase in S (defect creation) of 0.65 eV can be correlated to the activation energy of ≈ 0.4 eV for hydrogen loss from the (i-p)a-Si:H stack. This also suggests the presence of weakly bonded hydrogen in the (p)a-Si:H films, which effuses out of the film stack at such low activation energy. When light and heat stress are applied together, similar hydrogen loss from (i-p)a-Si:H stack is observed, however, does not appreciably degrade iV_{OC} or increase S. This is an important result and departure from direct correlation between hydrogen loss and defect creation. This perhaps indicates additional defect chemistries or annealing that might be occurring in the presence of light requiring further detailed defect measurements.

The full SHJ cell structure used for this project is depicted in Fig.1(d). SHJ cells with an initial V_{OC} ≈ 700 mV were fabricated and subjected to similar ALT stress conditions. Cell V_{OC} is found to degrade the most under dark heat stress and is confirmed by observed hydrogen migration out of the (i-p)a-Si:H stack. However, hydrogen cannot escape from the cell stack, it accumulates near the (p)a-Si:H/ITO contact interface, where ITO acts as a barrier preventing hydrogen loss. Furthermore, light-heat combined stress does not degrade V_{OC} appreciably, confirming the occurrence of a defect annealing process.

4. Table of Contents:

5. Background:

Silicon heterojunction solar cells (SHJ) are fabricated using multiple thin (5 – 10 nm) amorphous Si layers (intrinsic a-Si:H for Si surface passivation and doped a-Si:H for junction formation and back surface field (BSF))[1,2] and represented a departure from traditional diffused homojunction cells. These cells have since become the focus of international research efforts due to attractive qualities like high power conversion efficiencies through improved open circuit voltage (V_{OC}), low processing temperatures, and symmetric device structure for bifacial configuration. Record solar cell efficiency (≈27%)[3] and V_{OC} (≈750 mV)[4] for single junction Si solar cells are reported using SHJ structures. However, such high efficiency heterostructures have also shown higher degradation rate in fielded photovoltaic (PV) modules compared to standard diffused junction Si modules.[5,6,7] Standard diffused junction c-Si modules show an approximate rate of degradation of 0.5% per year, due to losses in short circuit current density (J_{SC}) and fill factor (FF). In contrast, many studies find degradation rates for SHJ modules to be around 1% per year[8,9], and higher rate of performance decline is dominated by nonlinear V_{OC} loss, a trend not observed in other silicon cell technologies.[5,6] This limits SHJ technology's market acceptance despite its record efficiencies. Improving PV device stability has been shown to greatly decrease the LCOE. A previous DOE report states that reducing efficiency degradation rate from 0.75% per year to 0.2% per year and increasing module lifetime from 30 years to 50 years greatly reduces efficiencies needed to reach grid price parity, as well as increases the allowed module cost per watt.[10] Decreasing module degradation rate and increasing lifetime are as important to reaching grid price parity as increasing module efficiency.[11] Therefore, many groups have investigated stability of SHJ passivation over the last few decades to understand the V_{OC} loss mechanism.

Studies focusing on degradation of (i)a-Si:H by itself [as shown in Fig.1(a)] have shown light-induced degradation of Si surface passivation for relatively thick (50 nm) i-layers[12,13], commonly referred to as the "Staebler-Wronski" effect. Similar metastable degradation has also been reported on thin (10 nm) (i)a-Si:H passivation layers, where the passivation is shown to completely recover by annealing at 300°C for 5 mins.[14] However, an uncapped i-layer (not protected by a following layer such as doped a-Si:H or ITO) may not mimic the encapsulated environment under which an operable cell would function. While these studies provide useful insight into passivation changes from light and heat stress, observations cannot be incontestably applied to full cells as there is no comparable degradation data on samples with subsequently deposited doped and ITO layers.

Si surface passivation structures are reported to degrade differently for (i)a-Si:H and after deposition of overlying doped a-Si:H layers. Passivation from only (i)a-Si:H can degrade or improve with light illumination time, depending on the process conditions and a-Si:H bonding structure, while (i-p)a-Si:H stack passivation improves, and (i-n)a-Si:H stack passivation degrades with light exposure.[15] Such light-induced kinetics and passivation improvement for (i)a-Si:H and the (i-p)a-Si:H stack are explained in terms of interface charging effect, likely changing the field-effect passivation. The effect of heat on (i)a-Si:H, as well as (i-p)a-Si:H and (i-n)a-Si:H stacks by means of thermal annealing is reported to cause changes in passivation quality opposite to the light-induced effect. The (i)a-Si:H and (i-n)a-Si:H stack passivation improves with thermal annealing up to ~ 280°C,

while (i-p)a-Si:H stack passivation degrades at temperature > 200°C.[16] These studies suggest that the changes in interface passivation strongly depend on the specific SHJ passivation layer structure and stress conditions.

In full SHJ cell configuration, several groups reported V_{OC} and performance improvement under light soaking,[17,18] which is enhanced by application of forward bias[19] and/or an optimum temperature.[20] But the cells exhibit V_{OC}-driven performance loss when heated to 160°C even for a short duration of 5 mins.[21] In contrast, SHJ modules weathered for 10 years in the field have shown unambiguous degradation-related defect formation at the a-Si:H/c-Si interface.[22] Theory predicts that Si–H bond breaking followed by drift of hydrogen atoms away from the interface causes additional defect formation.[23,24] Therefore, it is imperative to understand the role, kinetics and bonding configuration of interface hydrogen and their correlation to the electronic properties (i.e., surface passivation and V_{OC}) of the SHJ passivation stack.

6. Project Objectives:

The objective of this project is to identify the V_{OC}-degrading layer(s), interface(s), and stressors in SHJ solar cells to devise mitigation strategies. It is hypothesized that hydrogen in surface passivating (i)a-Si:H and/or HJ forming doped a-Si:H layers plays a crucial role, causing additional defect recombination in SHJ solar cells and V_{OC} degradation in fielded SHJ modules. This project develops an in-situ characterization method to decipher and quantify hydrogen microstructural changes in a-Si:H passivated Si surfaces during exposure to different degradation stressors (light, heat, and combined heat and light). These in-situ measured parameters are correlated to ex-situ measured changes in τ_{eff}, iV_{OC} and cell V_{OC} under similar ALT conditions. The final goals of this project are to provide a critically needed understanding of V_{OC}-driven SHJ cell performance loss mechanism and establish a causal relation to guide development of mitigation pathways. To achieve the stated goals, different symmetric SHJ passivation stacks [as shown in Figs. 1(a), (b), and (c)] are fabricated, characterized, analyzed, and exposed to different ALT stressors to distinguish the effect of different stress conditions on each individual layer(s)/interface(s). Consequently, the project is broadly categorized in following four major tasks.

Task 1: Symmetric SHJ surface passivation using intrinsic and doped a-Si:H layers
Task Summary: The goals of this task is to achieve effective Si surface defect passivation using symmetrically deposited, thin (≈ 10 nm) (i)a-Si:H, (i-p)a-Si:H and (i-n)a-Si:H stacks by plasma-enhanced chemical vapor deposition (PECVD). Depositing these symmetric structures is necessary for isolation of the (i)a-Si:H layer, as well as the (i-p)a-Si:H heterojunction and (i-n)a-Si:H BSF, to observe the influence of each individual component layer on passivation degradation. Surface passivation of each structure is assessed by τ_{eff}, measured by a Sinton quasi-steady state photoconductance (QSSPC) decay method. The injection-level dependent lifetime data are used to estimate the iV_{OC} at 1-sun illumination. Polished and textured n-type Si wafers are used for each passivation structures in the same run, thus achieving relevant and comparative information of τ_{eff}, iV_{OC} on both Si surfaces. The textured Si surface provides information that are relevant

to solar cell parameters, while polished Si surface is necessary to reduce light scattering for optical (FTIR and transmittance/reflectance) measurements, and for surface sensitive time-of-flight secondary ion mass spectrometry (ToF-SIMS) and x-ray photoelectron spectroscopy (XPS) characterizations with smooth interfaces. These structures are exposed to different ALT stressors (heat, light, and heat + light). *The milestones (1.2 and 1.3) for this task are to demonstrate τ_{eff} > 3 ms, iV_{OC} > 740 mV, and determine V_{OC} degrading stress conditions.*

Task 2: Development of in-situ FTIR for measurements under different temperature and light stresses of a-Si:H passivated Si surface
Task Summary: Modify an existing FTIR setup to illuminate and heat the samples inside a vacuum chamber. The set-up will have a temperature- and ambient-controlled transmission FTIR stage used for mounting samples. The geometry of the sample manipulator is ideally suited for exposing the sample to external illumination while recording infrared spectra. The FTIR spectra are recorded to identify different Si–H vibrational peaks associated with SiH, SiH_2, and SiH_3 in the a-Si:H films and at the a-Si:H/c-Si interface. The changes in hydrogen bonding structures are measured in-situ under heat and light exposure to decipher the hydrogen kinetics. *The milestones (2.1 and 2.2) for this task are to demonstrate sample heating up to 400^{o}C, and perform in-situ measurements under heat and light illumination.*

Task 3: SHJ Cell fabrication and ex-situ characterization of hydrogen distribution in a-Si:H and at the interfaces, τ_{eff}, iV_{OC} and cell V_{OC}
Task Summary: SHJ solar cells (pi/Si/in) are fabricated on n-type Si wafers with front-side deposited transparent conductive oxide (TCO) and metal grid fingers and back-side TCO and a full area metal contact. These SHJ cells are subjected to heat and light stress experiments (1-sun illumination and at < 150^{o}C) under similar conditions to the symmetric SHJ passivation structures in Task 1. Detailed ex-situ characterization of cells as a function of stress time includes dark and light current-voltage (I-V) curves, and elemental depth profiling by ToF-SIMS to elucidate hydrogen distribution and migration and/or impurities in the cell stack that are beyond the detection limit of FTIR. *The milestones (3.1 and 3.2) for this task are to demonstrate cell V_{OC} > 730 mV and identify changes in chemical species after different ALT stresses.*

Task 4: Develop a predictive model for SHJ cell degradation based on hydrogen kinetics for mitigation of V_{OC}-driven degradation pathways
Task Summary: Activation energies are calculated using results from in-situ FTIR measurements taken from symmetric samples while exposed to light and/or heat stress. In this task, changes in hydrogen bonding structure and concentration are correlated with passivation degradation, quantified by τ_{eff}, iV_{OC} and cell V_{OC} in SHJ structures under different stress conditions. *The milestone (4.1) for this task is to determine the activation energies associated with hydrogen evolution and correlate them to the degradation of t_{eff}, iV_{OC}, and cell V_{OC}. Based on the Tasks 1 – 4, the end of project goal is to explain pathways for V_{OC}-driven degradation in SHJ structure (degradation model) and disseminate results in two publications.*

7. Project Results and Discussion:

Task 1: Si surface passivation and HJ formation using intrinsic and doped a-Si:H layers

Milestone 1.2: Si surface passivation by intrinsic a-Si:H and obtain τ_{eff} > 1 ms and iV_{oc} > 730 mV
Milestone 1.3: Si HJ passivation with intrinsic and doped a-Si:H layers with initial τ_{eff} > 3 ms and iV_{oc} > 740 mV; define stress condition(s) for passivation degradation

Summary: The surfaces of silicon wafers are passivated by (i)a-Si:H grown by PECVD and optimized to achieve effective Si surface defect passivation. Both textured and polished wafers show similar passivation quality with τ_{eff} ≈ 1 ms at (i)a-Si:H thickness of 10 nm. Employing a stack layer process, where the plasma was briefly (60 s) interrupted at halfway stage (5 nm) of deposition and a post growth annealing at 300°C for 30 mins, τ_{eff} > 2ms and iV_{OC} ≈ 740 mV are achieved. *These values exceed the Milestone 1.2 of τ_{eff} > 1 ms and iV_{oc} > 730 mV.* Integrating the annealed stack i-layer passivation with the doped (p-type and n-type) a-Si:H layers, the iV_{OC} of 725 mV and 740 mV are achieved for (i-p)a-Si:H and (i-n)a-Si:H stacks, respectively. *This met the Milestone 1.3 for (i)a-Si:H and (i-n)a-Si:H stack passivation of iV_{OC} = 740 mV, but falls short by 15 mV for (i-p)a-Si:H stack.* After establishing the state-of-the-art passivation quality, the symmetric SHJ passivation structures were subjected to different combination of dark, light, and heat stress conditions for ≈1000 hrs. The iV_{OC} of thin (10 nm) i.a-Si:H passivation itself (without any overlying doped a-Si:H layers) show a complex degradation behavior with partial metastability. However, iV_{OC} of (i-p)a-Si:H stack passivated samples degrade at much faster rate (> 3 times faster) under heat than any other stress conditions or (i-n)a-Si:H stacks. *This suggests heat stress of (i-p)a-Si:H HJ is one of the primary contributors of V_{OC} degradation.*

Subtask 1.A: *Si Surface passivation by (i)a-Si:H*

The deposition of (i)a-Si:H on clean Si surfaces plays the most critical role to achieve effective passivation of surface defects. This requires development of Si wafer surface cleaning process and optimization of plasma process parameters of (i)a-Si:H.

Two different n-type Si surface types, polished float-zone (FZ) and textured Czochralski (Cz), were used for surface passivation. The n-type, textured Cz c-Si wafers used were 120 µm thick with resistivity of 2 – 5 Ω·cm, and the n-type polished FZ c-Si wafers used were 225 µm thick with similar resistivity of 4 – 5 Ω·cm. Textured wafers are used here to maximize light absorption and mimic SHJ cell conditions, and are needed to accurately investigate surface passivation quality via QSSPC. Polished wafers are used to estimate film thickness by fitting experimental reflectance and transmittance spectra,[25] and for characterization by FTIR, XPS and ToF-SIMS.

The wafers were cleaned/textured using the processes developed by IEC under previous SETO-funded program.[26] The processes are briefly described below:

Process 1: (Preparation of textured clean n-type Si wafer): 10% HF for 1 min + 1 min Si etching in a mixture of (1:100) HF and nitric acid (HNO_3) (HNA etch) + 10% HF for 1 min + 30 mins texture etch in 1% tetramethylammonium hydroxide (TMAH) at ≈ 75°C + 5

mins ultrasonication in methanol + 5 mins Piranha oxidation + 10% HF steps with DI water rinse between each step.

Process 2: (Preparation of polished clean n-type Si wafer): 5 mins ultrasonication in acetone + 5 mins ultrasonication in methanol + 5 mins Piranha oxidation + 10% HF steps with DI water rinse between each step.

The cleaned Si wafers were loaded into a direct current (DC) PECVD reactor immediately after the final HF step. Both polished and textured Si wafers were used concurrently in each deposition run to enable accurate comparison between electronic and spectroscopic measurements. Our baseline (i)a-Si:H process condition as follows: substrate temperature of 200°C, deposition pressure of 1250 mTorr, SiH_4 flow rate of 10 sccm, H_2 flow rate of 25 sccm, and varying dc plasma current of 30 – 150 mA, resulting in the power variation of ≈ 12 – 60 W.

Fig. 2 shows the τ_{eff} values at an excess carrier concentration (Δn) of 10^{15} cm^{-3} as a function (i)a-Si:H thickness. Here the τ_{eff} increases sharply to ~ 1 ms as the (i)a-Si:H thickness reaches ≈ 10 nm. This suggests that the minimum thickness of the (i)a-Si:H needs to be ≈ 10 nm to achieve optimum surface passivation quality. Fig. 2 also clearly shows that similar passivation quality (τ_{eff}) can be achieved for both polished FZ and textured Cz Si wafers, signifying relevance and compliance of electronic passivation quality measurements taken from textured c-Si with the optical and structural characterization taken from polished Si wafers.

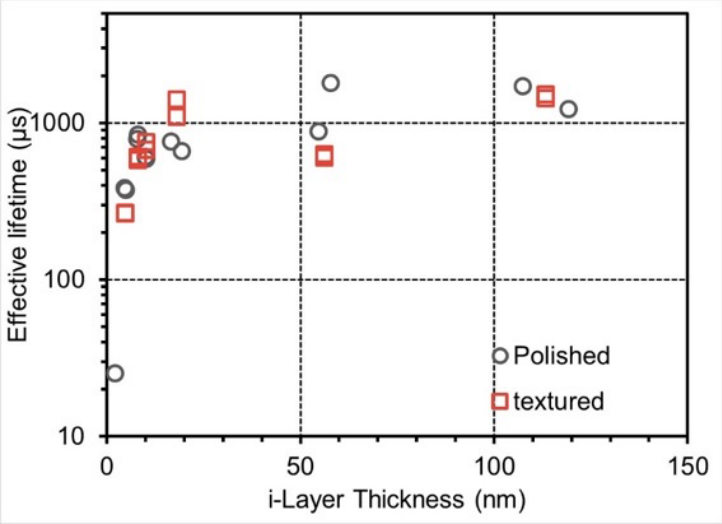

Fig. 2. Surface passivation quality (τ_{eff} at $\Delta n = 10^{15}$ cm^{-3}) as a function of i-layer thickness. The i-layers are deposited with dc plasma current of 120 mA on both surfaces of the wafers as stack layer (i.e., the plasma was turned off and on at the halfway stage of each thickness).

Fig. *3* shows the variation of (a) τ_{eff} and (b) iV_{OC} as a function of DC plasma current during (i)a-Si:H deposition in two different ways: a) continuous deposition (termed as “single”) for a desired duration to achieve ≈ 10 nm thick film and b) an interrupted deposition, where the plasma power was briefly turned off and then on again after 60 seconds at the halfway stage (2x 5 nm thickness, termed as “stack”). A “stack”, bi-layer (i)a-Si:H structure is often

employed in literature and is recognized as the most effective method to achieve superior surface passivation.[27,28] The red triangles represent the τ_{eff} and iV_{OC} values after the post-deposition annealing of the stack layer at 300°C for 30 mins. It is noticed that the lifetime varies by almost an order of magnitude in τ_{eff} and by about 100 mV in iV_{OC} in the studied range of plasma current (30 – 150 mA). The "stack" layer passivation was found to be superior to the "single" layer with ≈ 20 mV improvement in iV_{OC} at all plasma current conditions. Post deposition annealing further improves τ_{eff} to > 1 ms for the plasma current of 120 mA, leading to up to additional 20 mV improvement in iV_{OC} to reach iV_{OC} = 738 mV. *These values exceed expectations for Milestone 1.2.*

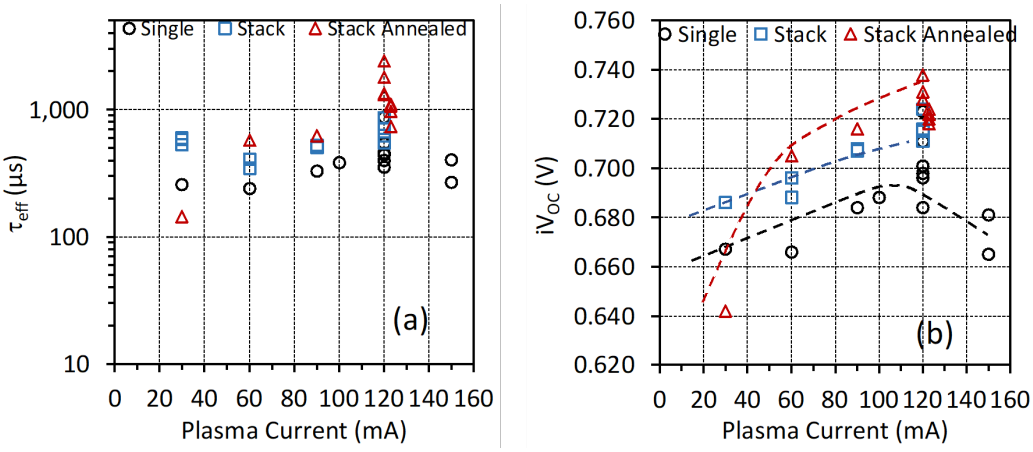

Fig. 3. τ_{eff} values after surface passivation of textured c-Si wafers using different a-Si:H structures: single (circle), stack (square) and annealed stack (triangle) deposited with varying plasma current. (b) iV_{OC} obtained from QSSPC from the same set of samples as (a). Dashed lines are shown only as a guide.

To gain further insight into the improvement of passivation quality, the hydrogen bonding behavior in deposited (i)a-Si:H layers was investigated by FTIR on the companion polished wafer samples. Fig. *4*(a) plots the evolution of FTIR absorbance in the wavenumber range of 1800 – 2300 cm^{-1} corresponding to the Si-H and Si-H_2 stretching vibrational peaks as a function of (i)a-Si:H thickness. The distinct peaks at approximately 2000 cm^{-1} and 2080 cm^{-1} can be identified, which are often referred to as low stretching mode (LSM) and high stretching mode (HSM), respectively.[29] It shows that the hydrogen bonding microstructure is changing as the film gets thicker, where the HSM peak is predominant at 2.5 nm and the LSM peak is predominant at 20 nm. This suggests that the a-Si:H films nucleate with HSM microstructure at the initial stage of deposition, which gradually changes to LSM microstructure as the film gets thicker.

Fig. *4*(b) shows the FTIR absorption coefficient in the wavenumber range of 1900 – 2200 cm^{-1} for the "single" ~10 nm thick (i)a-Si:H grown at different DC plasma current. The a-Si:H films deposited with plasma current of 30 mA show LSM as predominant and increase of plasma current increases HSM contribution with an associated decrease of LSM. Therefore, comparing these results with Fig. 3(b), it can be concluded that a-Si:H films with higher HSM provides better passivation quality with higher iV_{OC}. Comparison of single and stack a-Si:H layers deposited under same conditions with plasma current of 120 mA, shown in Fig. *4* (c), interestingly show reduction of LSM, with no discernible change in HSM for stack layer. This likely indicates that the "stack" layer (interruption of

plasma) promotes denser nucleation sites leading to better film coverage, as well as increased τ_{eff} and ≈ 20 mV increase in iV_{OC} compared to the "single" layer. Fig. *4*(d) shows that the hydrogen bonding microstructure does not appreciably change after post deposition annealing of the layers. But a uniform reduction of both LSM and HSM peak intensities is observed. Thermal annealing causes removal of some hydrogen and likely densifies the films. Therefore, it is determined that the Si-H microstructural measurements by FTIR can provide critical information of the Si surface passivation quality and iV_{OC}.

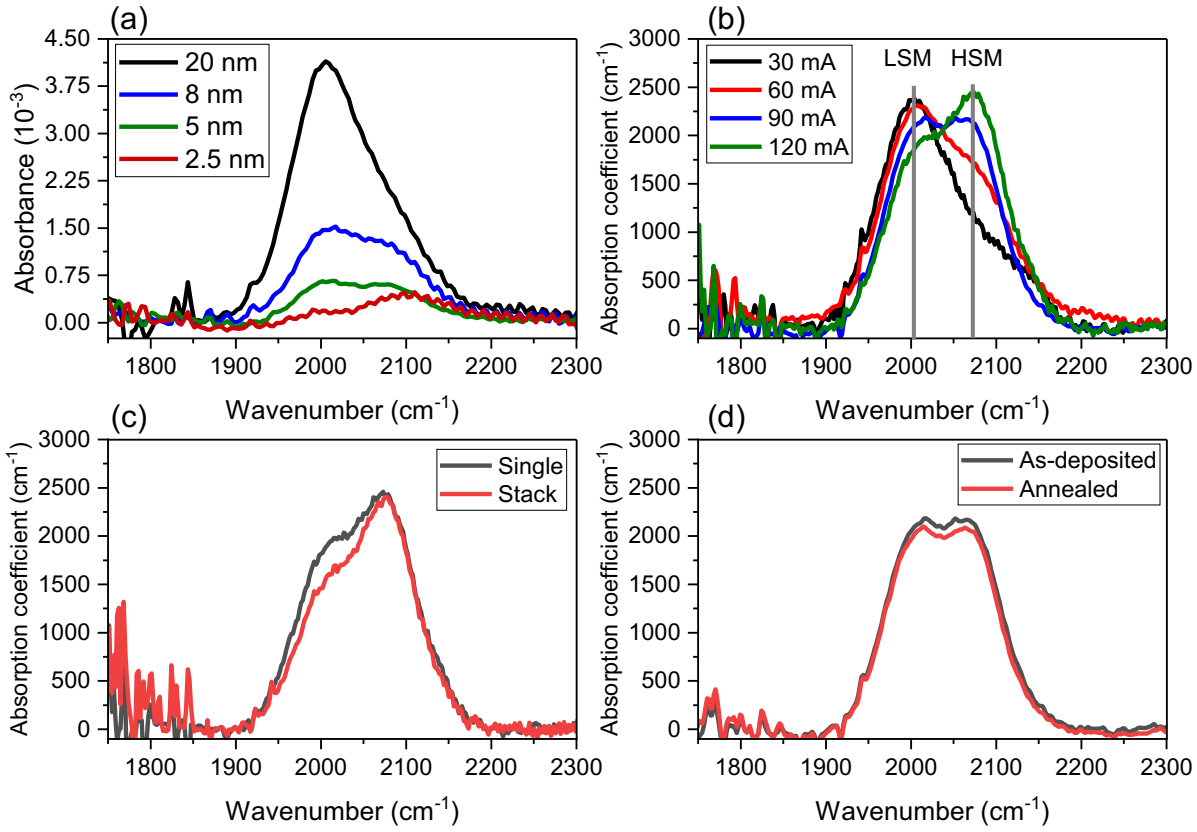

Fig. 4. (a) Si-H stretching vibrational peaks as a function of i-layer thickness. (b) for 10 nm thick a-Si:H films deposited at different dc plasma current. (c) comparison of FTIR peaks for 10 nm thick "single" and "stack" a-Si:H films deposited with 120 mA plasma current. (d) comparison of FTIR peaks for "as-deposited" and "annealed" 10 nm a-Si:H film deposited with 90 mA plasma current.

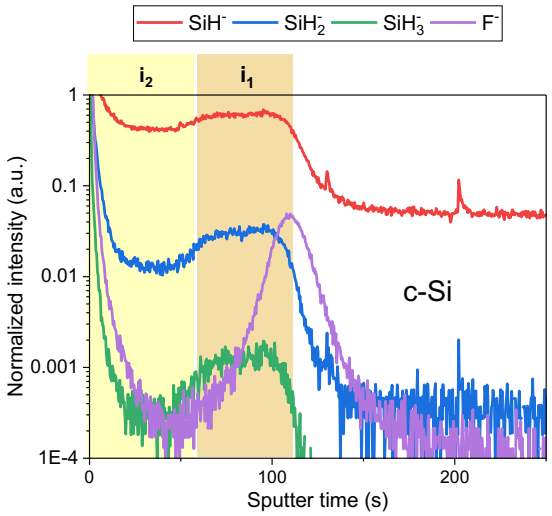

Fig. 5. Time-of-flight secondary ion mass spectrometric (ToF-SIMS) depth profile of a stack (i1+i2) i-layer deposited on n-type polished Si wafer. Approximate depths of each layer are denoted by highlighted areas.

The ToF-SIMS depth profiles provide hydrogen and other elemental distribution throughout the film. The ToF-SIMS analysis of a (i1+i2) stack passivated polished Si wafer was performed on a TOF.SIMS 5 instrument (ION-TOF USA, Inc.) equipped with a pulsed 30 keV BiMn cluster ion gun, Cs, and O_2 dual-source ion column for ultra-low energy sputtering, and low energy electron flood gun for charge compensation. For the depth profile, a 250 eV Cs^+ sputter ion beam with a 30 nA current was applied to create a 200μm × 200 μm area. The analysis area was 50 μm × 50 μm inside the sputtered crater. Figure 5 shows the negative ions of SiH^-, H^-, SiH_2^-, SiH_3^-, F^-, and SiF^- traces normalized with respect to Si_2^- signal as a function of sputter time (film depth). The F signal presumably appears due to residues of the HF cleaning step of the c-Si wafer surface and indicates the interface of c-Si wafer and the deposited a-Si:H film. This signal corresponds to a very small amount of fluorine (well below a monolayer), but because of high ionization cross-section, the peak appears to be very intense. The i1 layer deposited with dc plasma current of 120 mA at the Si interface clearly shows higher concentration of hydrogenated species than the i2 layer deposited with DC plasma current of 30 mA.

In summary, we found that Si surface passivation quality is related to the hydrogen bonding microstructure in the a-Si:H films and at the a-Si:H/Si interface. It appears that higher HSM improves τ_{eff} and iV_{OC} (Fig. *3* and Fig. *4*). The “stack” layer and post deposition annealing both improves τ_{eff} and iV_{OC}, but underlying change in hydrogen bonding microstructure is different. The stack layer reduces LSM, keeping the HSM to same level, while annealing reduces both LSM and HSM intensities and reduces hydrogen content in the film. Additionally, ToF-SIMS depth profiling shows that a higher hydrogen content closer to the (i)a-Si:H/c-Si interface improves initial passivation, observable through elevated iV_{OC} values.

Summarizing all of the previous reported results from optimization of each element allowed for the creation of a set of optimized deposition parameters. The first set of

parameters used throughout the beginning of this project are listed in Table 1 as “old i1” and “old i2” to represent each layer in a bi-layer structure. However, as the project period progressed, the passivation ability of our deposited i.a-Si:H layers was observed to be worsening as confirmed by decreasing τ_{eff} and iV_{OC} values compared to films deposited using the old set of parameters. Several adjustments to the PECVD system were made that had potential to affect the quality and reproducibility of the a-Si:H layers and required recalibration, such as changes in process control electronics, process gas cylinder, chamber cleaning, and electrode spacing. After all adjustments were made, new process conditions were established following the same optimization experiments as previously performed, and are reported in Table 1 as “new i1” and “new i2” layer. Fig. 6 summarizes the statistical changes in passivation quality from differing deposition conditions throughout the project. Each x-axis category represents a different (i)a-Si:H process, grouped into single layer, stack layer, and plasma deposition conditions (described in Table 1). The “new” i1+i2 condition clearly shows the highest iV_{OC} observed throughout the project, however, the spread of the data is larger than the “old” i1 + i2 condition. This indicates continued issues with reproducibility of the “new” condition, meaning further optimization is required to perfect the condition to allow for more consistent results.

Table 1: Different process parameters for (i)a-Si:H used in this project. The deposition time shown for each condition represent the time to grow 5 nm thick films.

Sample type	SiH_4 /H_2 gas ratio	Plasma current (mA)	Chamber pressure (mTorr)	Deposition Time (seconds)
Old i1	10/25	120	1250	24
Old i2		30		75
New i1	10/25	60	1750	20
New i2		30		70

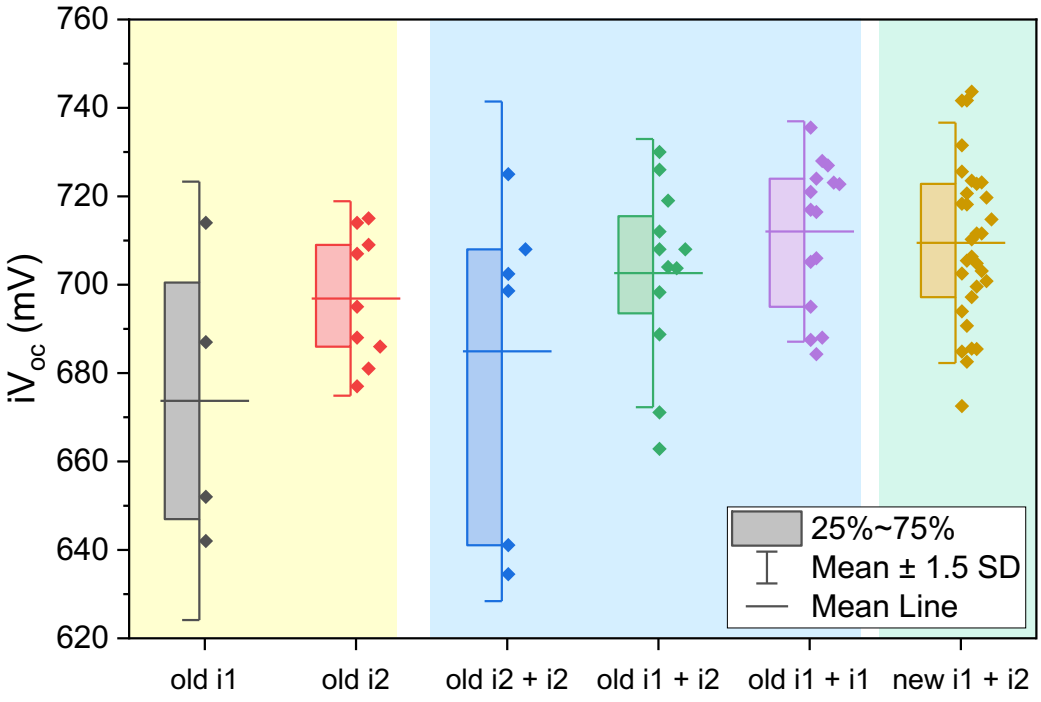

Fig. 6. Box-and-whisker plot of iV$_{OC}$ values obtained after Si surface passivated by 8 – 10 nm thick (i)a-Si:H with different layer structures and process conditions throughout the project period.

Subtask 1.B: *Si surface passivation by combined (i-p)a-Si:H and (i-n)a-Si:H layers stack*

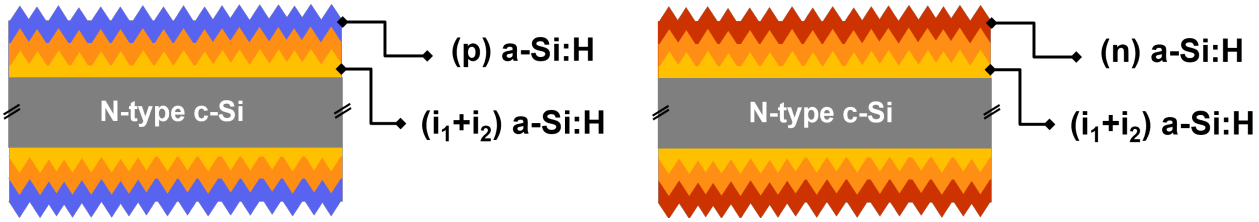

Fig. 7. Schematic structures of i-p (hetero-junction) (left) and i-n (BSF) stack (right) structures on polished n-type Si wafers. Different colors refer to different layers on the structure.

After establishing effective surface passivation by stack (i)a-Si:H i-layer, (i-p)a-Si:H and (i-n)a-Si:H stacks are deposited in symmetric structures, as shown in Fig. 7 on both textured and polished n-type c-Si wafers. The (p)a-Si:H layer is deposited on top of the stack (i)a-Si:H on both surfaces at 200°C and adding 1.5% B_2H_6 (B_2H_6/SiH_4 flow ratio = 0.015) dopant gas; the process is otherwise similar (i)a-Si:H process condition. Conversely, the (n)a-Si:H layer is deposited at 250°C and adding 1% PH_3 (PH_3/SiH_4 flow ratio = 0.01) dopant gas to the (i)a-Si:H process parameters.

Fig. 7 shows passivation results through iV_{OC} for i/doped symmetric structures throughout the project period. The "old" i1+ i2 and "new" i1+i2 condition labels refer to the parameters detailed in Table 1. Improvement of the underlying (i)a-Si:H layer passivation, as discussed previously under Milestone 1.2, was shown to also improve the overall passivation when doped layers were applied. While the mean iV_{OC} for the "new" i1 + i2 condition is slightly lower than the "old" i1 + i2 condition, the new condition provides a better / more reproducible iV_{OC} once doped layers are added for both the (i-p)a-Si:H and (i-n)a-Si:H symmetric structures. Another observation is that the maximum $iV_{OC} \approx 740$ mV is achieved by (i)a-Si:H and (i-n)a-Si:H passivation stack, while highest iV_{OC} of (i-p)a-Si:H stack passivation is 725 mV. *This meets Milestone 1.3 of initial $iV_{oc} > 740$ mV for (i)a-Si:H and (i-n)a-Si:H stack passivation, but falls short by 15 mV for (i-p)a-Si:H stack.*

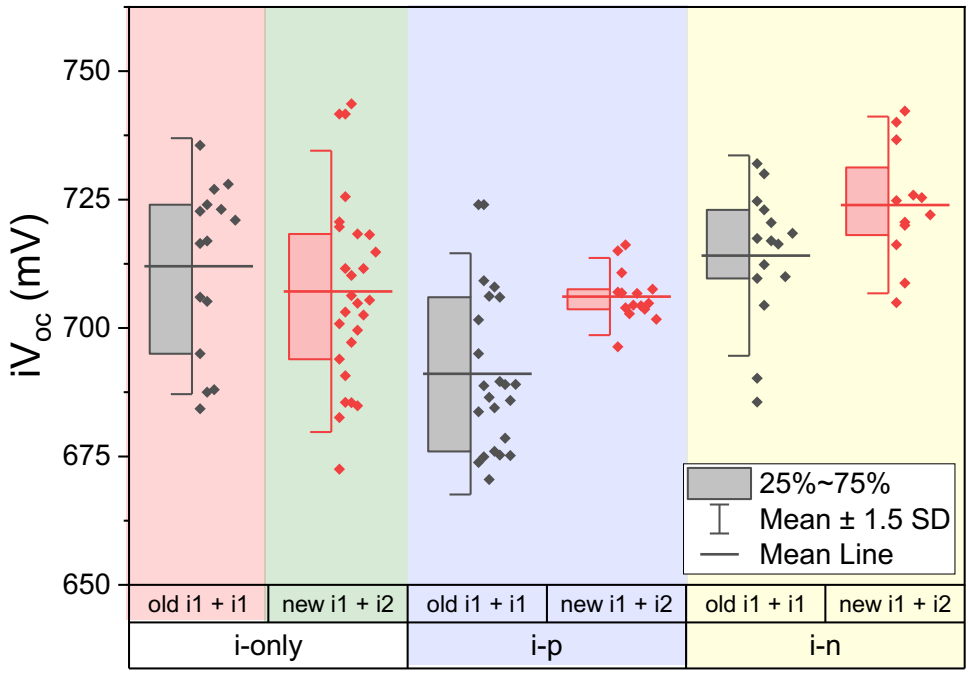

Fig. 8. Box-and-whisker plot of iV_{OC} from c-Si symmetrically passivated with (i)a-Si:H (i-p)a-Si:H, and (i-n)a-Si:H stacks throughout the course of the project period.

Subtask 1.C: *Identifying stress condition(s) and layer stack(s) that causes passivation degradation*

Symmetrically passivated SHJ structures are systematically tested using accelerated lifetime testing (ALT) to comprehend degradation pathways of each layer and/or combination of layers before analyzing the full cell. The ALT process involved applying

differing combinations of 1-sun light and constant heat (120°C) to accelerate the aging process of the samples. The pod system used at the IEC is shown in Fig. *9*, where Fig. *9* (a) shows the separate lighting allowing for individual testing of heat and light, and Fig. *9*(b) shows the full system with four separate Ar purged pods. The full list of conditions tested is outlined in Table 2. Each condition will be referred to by its listed abbreviation in the following discussion of results.

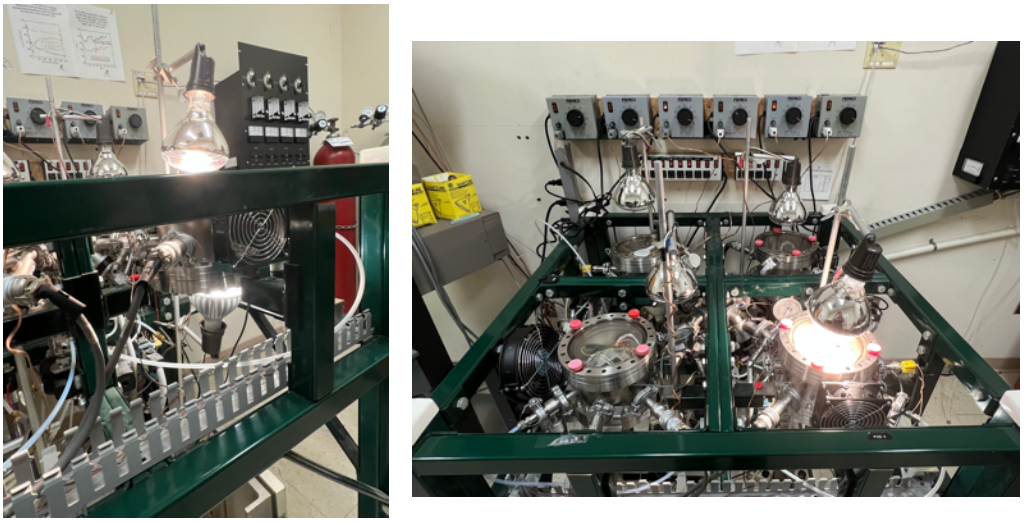

Fig. 9. (a) Individual pod used for ALT with separate top infrared heat and bottom white light lamp. (b) Four ALT pod system used at the IEC, where each chamber is separately vacuum pumped and purged with Ar gas during the stress experiment.

Table 2: Different stress and ambient conditions applied to the symmetric SHJ passivated Si wafers.

Condition	Light	Temperature	Atmosphere
C (no stress)	Dark	30˚C	Medium vacuum (10^{-1} mTorr)
D (no stress)	Room light	30˚C	N_2 desiccator with relative humidity ≈ 20%
L	1-sun white light	30˚C	Ar
H	Room light	120˚C	Ar
LH	1-sun	120˚C	Ar

Stress exposure of symmetric (i)a-Si:H (10 nm) passivated c-Si

The c-Si wafers passivated by just (i)a-Si:H are investigated via ALT and discussed here first to establish any changes occurring at this layer which sits closest to the wafer surface. The (i)a-Si:H layer is often hypothesized to be the main source of SHJ cell V_{OC}

loss, so establishing the degradation mechanisms of (i)a-Si:H layers before adding additional layers is crucial. Fig. 10 shows iV_{OC} loss trends under different stress conditions for a total of approximately 250 hours, followed by subsequent re-annealing at 300°C for 30 minutes. Results from Fig. 10 (a) show that the samples exposed to the D and L conditions monotonically degrade over time and partially recover iV_{OC} after re-annealing. LH and H stress show a drastic degradation of iV_{OC} for the first hour of stress, and then a slight increase in iV_{OC} during stresses. However, a thermal re-annealing after H and LH stress samples does not show any iV_{OC} recovery, unlike for the samples exposed to L and D stress. It is to be noted that all stress conditions result in a rapid drop of iV_{OC} for the first 15 hrs, except for the sample stored in medium vacuum (C condition). This indicates some rapid changes at the (i)a-Si:H surface are occurring in non-vacuum ambient. X-ray photoelectron spectroscopy (XPS) measurement is performed to understand changes in the surface chemical structure.

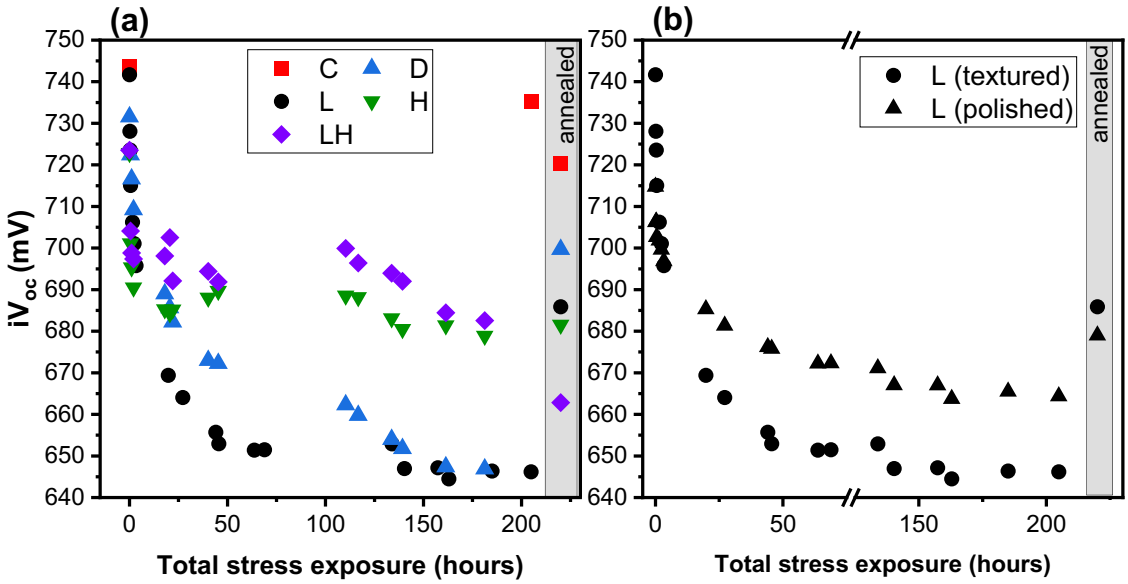

Fig. 10. iV_{OC} degradation observed over approximately 200 total hours for 10 nm thick (i)a-Si:H passivated c-Si samples. (a) Shows results from samples deposited on textured wafers only for all stress conditions, (b) compares samples deposited on polished and textured wafers for the L stress condition only. iVoc after annealing is denoted in shaded column.

Fig. 10 also shows a different degradation behavior for different stress conditions beyond the initial 15 hrs of stress. The presence of heat in stress exposure stabilizes or perhaps improves iV_{OC}, while light stress shows a non-linear degradation of iV_{OC}. But this light-induced degradation appears to be metastable and can be fully recovered by thermal annealing, a phenomenon commonly known as Staebler-Wronski effect. ToF-SIMS depth profiling was performed to investigate potential changes in chemistry within the i.a-Si:H layers and at the (i)a-Si:H/c-Si interface as a result of applied stress. The resulting depth profiles in Fig. 11 show no observable differences in distribution of hydrogen-related species between samples exposed to different stress conditions (D, H, LH). Therefore, it

is postulated that changes in iV_{OC} for i-layer passivated Si are not due to changes in Si–hydrogen bonding chemistry.

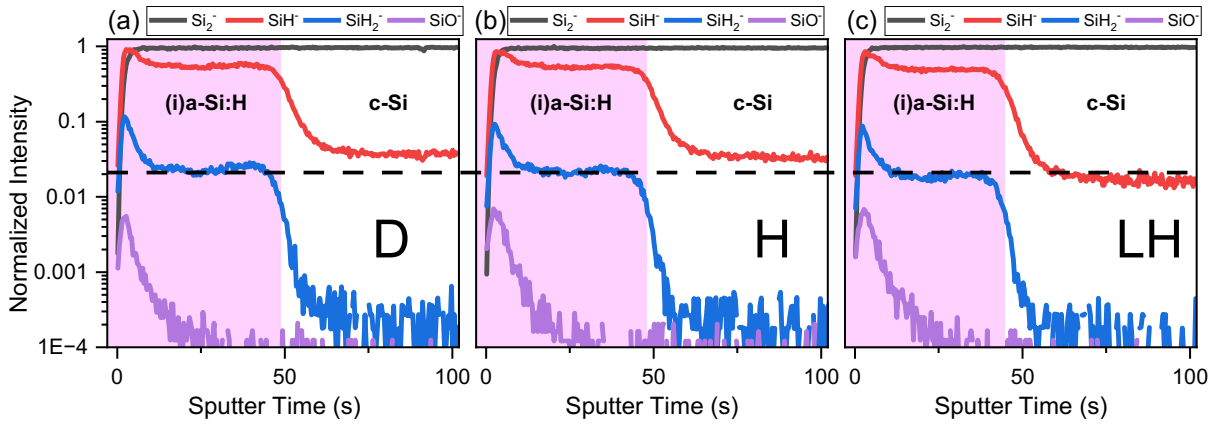

Fig. 11. ToF-SIMS depth profiles taken from samples with only (i)a-Si:H layers deposited, after different stress (D, H, LH) exposures for 250 hrs.

Fig. 12 (a) shows the changes in Si 2p peaks recorded with XPS before and after each stress condition was applied. Increase in intensity of the higher binding energy peak around 103 eV indicates oxidation of the (i)a-Si:H surface via formation of SiO_X. Fig. 12 (b) zooms into the oxidized Si 2p spectral region after approximately 15 hours of stress exposure, and Fig. 12 (c) shows this binding energy region after the full stress exposure period had elapsed. A spectrum taken from a sample with the same (i)a-Si:H layers immediately after deposition (labeled as “As-deposited”) is also included for comparison. The rate of oxidation is observed to be faster in samples exposed to LH and H stresses, as observed by the increased peak intensity of the corresponding spectra after 15 hours. However, after the full stress exposure period has elapsed, all stress conditions exhibit similar intensities of the SiO_X peak. Therefore, the initial rapid drop in iV_{OC} observed in all samples shown in Fig. 10 is likely due to surface oxidation during stress exposure, regardless of the rate at which this oxidation is occurring.

XPS depth profile following sputtering with Ar^+ is presented for the sample under the D condition in Fig. 12 (d) to realize the depth of oxidized layer. The SiO_X peak disappears nearly completely within the top 2 nm of film. These data show that surface oxidation drastically affects the thin (i)a-Si:H matrix as well as the passivation quality. Future studies concerning (i)a-Si:H degradation without an additional capping layer would need to consider inevitable oxidation and/or performing the stress experiments without air exposure.

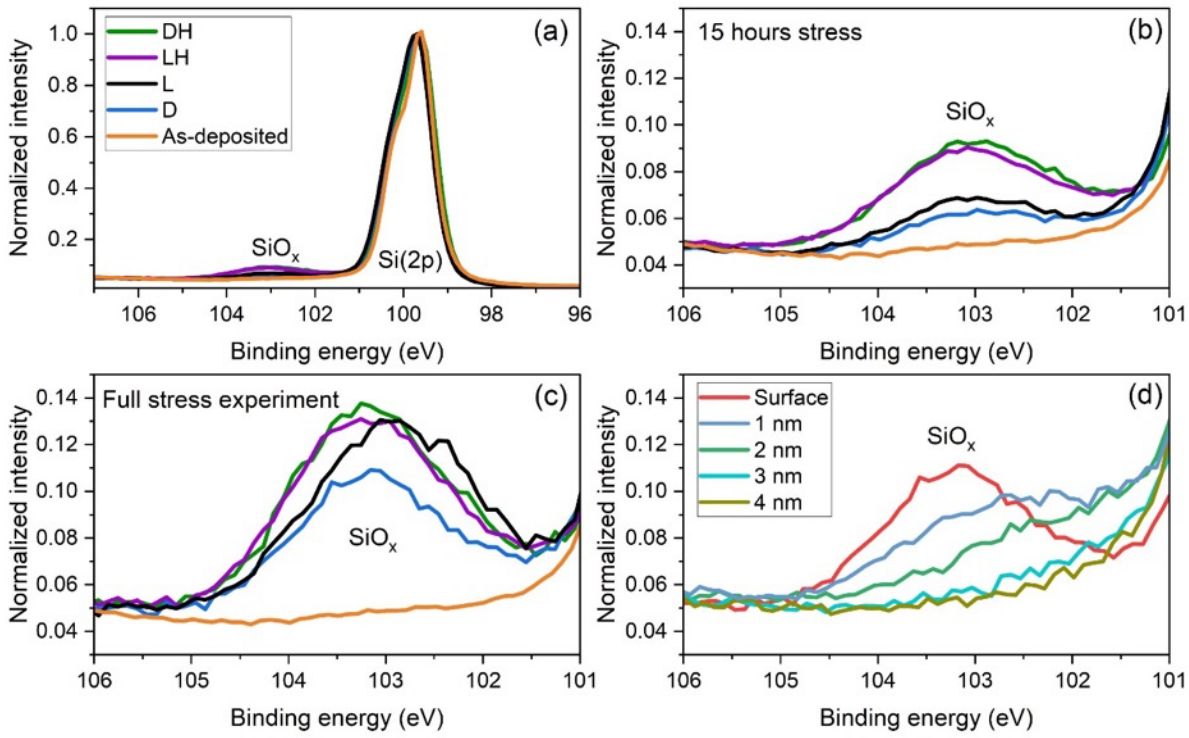

Fig. 12. X-ray photoelectron spectra of the Si(2p) region taken from samples exposed to different stresses. Intensity was normalized to the Si (2p) bulk peak. (a) Shows the full area of interest for the spectra collected after ~ 15 hours of stress and as-deposited condition, (b) Enlarged region of the SiO_X peak only. Spectra collected from the same samples after the full ALT period (250 hrs) are shown in (c). Photoelectron spectra at different sputter depth are shown in (d) for the sample exposed to D stress, showing SiO_X peak diminishes to negligible level at a depth of ~ 2 nm.

Stress exposure of symmetric (i-p)a-Si:H heterojunction stack passivated Si

After the (i)a-Si:H layer, the (i-p)a-Si:H and (i-n)a-Si:H symmetric stack structures were subjected to the same ALT process to determine the influence of the doped layers on the previously reported results for just the (i)a-Si:H layer. Testing the doped layers in these symmetric structures additionally allowed for isolation the influence of each dopant on the overall passivation degradation. Fig.12 shows the changes in iV_{OC} during the four different stress conditions. The LH and L conditions [(Fig. 13 (b) and (d)), respectively] degrade at a similar rate (4 – 9 mV after ≈1000 hrs) as the D condition [Fig. 13 (a)], implying a minimal change in iV_{OC} in presence of light. Whereas the sample under H stress degrades 3 – 5 times faster (26 mV after ≈1000 hrs) [Fig. 13(c)] than the other stress conditions. This contrasts with the degradation behavior observed in Fig. 10, where both H and LH stress degrade similarly for the (i)a-Si:H only passivated samples.

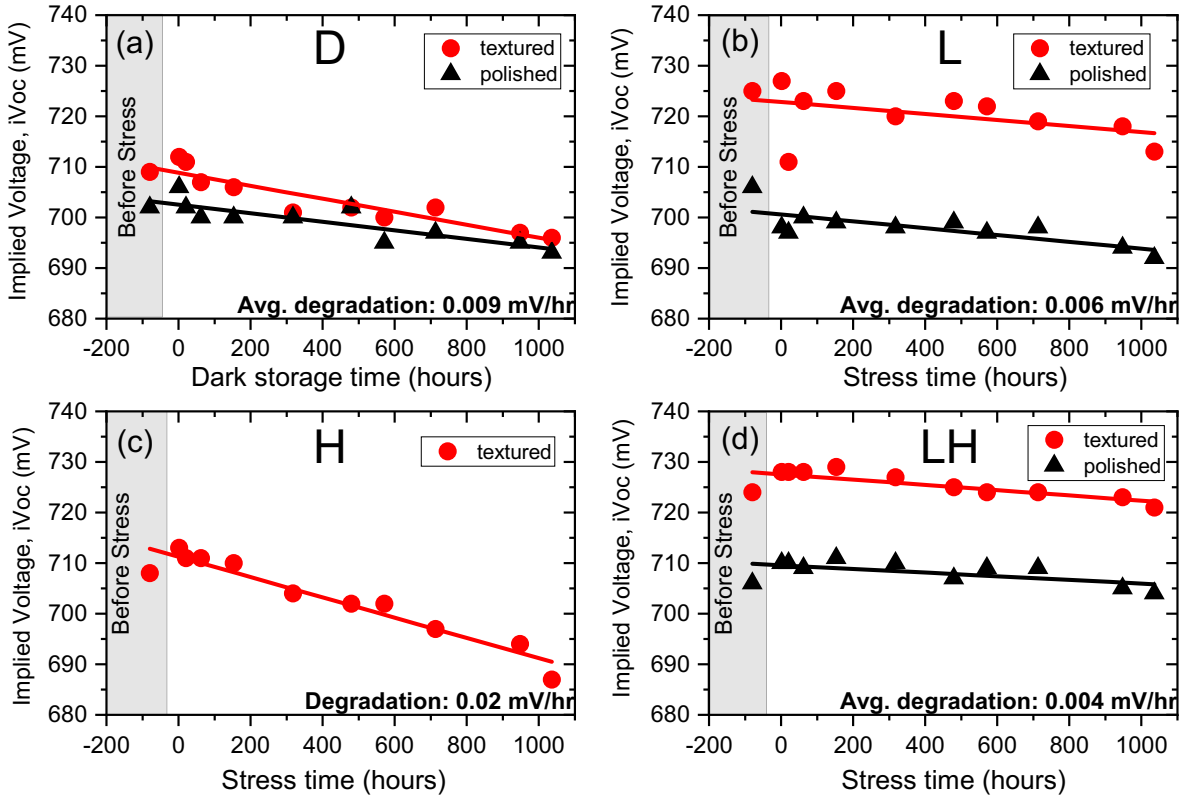

Fig. 13. iV_{OC} of symmetric (i-p)a-Si:H hetero-junction passivation resulting from the application of four different stress conditions: (a) D, (b) L, (c) H and (d) LH.

To further investigate iV_{OC} degradation of (i-p)a-Si:H stack symmetric structures, the ToF-SIMS depth profiles were taken after different stress exposures for ~ 1000 hrs. In Fig. 14, depth profiles of three samples exposed to (a) D, (b) H, and (c) LH are shown. The trend of hydrogen loss from (p)a-Si:H is most clearly visible when following the SiH_2^- depth profile, where the D condition profile has the most intensity of this curve closest to the surface, then the profile after H stress shows less intensity, and finally the LH stress condition shows the least intensity for this curve. The downward slope of this curve for the LH condition indicates that the SiH_2 content is lower towards the surface of the layer. Loss of higher order SiH_3^- is also visible through a lowered intensity of these profiles. The (p)a-Si:H layer is losing hydrogen at a differing rate based on the stress condition. Observed hydrogen loss in these (i-p)a-Si:H stack structures could be attributed to the properties of the (p)a-Si:H layer, as these hydrogen loss trends are not observed in the samples with (i)a-Si:H only, discussed previously. This indicates the loss of hydrogen from the heterojunction passivation stack as the likely reason for higher rate of degradation under H stress. However, the lowest rate of iV_{OC} degradation under LH stress [Fig. 13(d)] cannot be corroborated by obvious loss of hydrogen observed in Fig. 14(c). We presume this might indicate some sort of defect anneal and/or dopant activation that are occurring under illumination, as reported in some literature.[17,18,21]

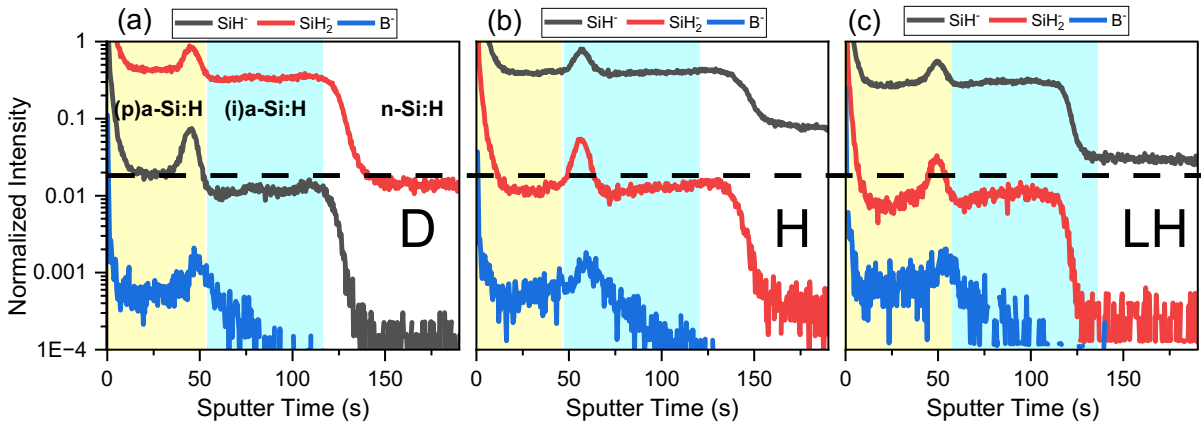

Fig. 14. ToF-SIMS depth profiles of (i-p)a-Si:H stack on Si, where (a) was taken from the sample exposed to the D condition, (b) the H condition, and (c) the LH condition. These depth profiles were taken after 1000 hours of stress exposure.

Stress exposure of symmetric (i-n)a-Si:H BSF stack passivated Si

A total of 8 symmetric stack of intrinsic & n-type doped a-Si:H layer (i-n)a-Si:H structures were fabricated on polished and textured Si wafers (4 textured and 4 polished Si wafers). The thicknesses of intrinsic and n-type doped layers were 10 nm and 30 nm, respectively. These hetero-contact BSF stacks are also subjected to the 4 different stress conditions as described above for the (pi) stacks. Fig. 15 shows the changes in iV_{OC} of symmetric (i-n)a-Si:H stacks after (a) D, (b) L, (c) H, and (d) LH stress conditions were applied. After ≈1000 hours, all stress conditions show similar minimal degradation of iV_{OC} (4 – 7 mV) as the storage (D) samples. More importantly, the H stress of (i-n)a-Si:H stacks does not exhibit higher rate of degradation. This contrasts with the (i-p)a-Si:H stack, where 3 – 5 times faster degradation is observed. The ToF-SIMS depth profiles shown in Fig. 16 for (a) D, (b) H, and (c) LH do not show any appreciable change in the SiH_x-profiles from the n-layer, but perhaps indicate some hydrogen redistribution in the stack under H and LH stress. *This result indicates that the change in Si–H bonding and iV_{OC} degradation is associated with the (p)a-Si:H layer in the (i-p)a-Si:H heterojunction stack under heat stress and meet the Milestone 1.3 of defining layer and stress condition responsible for V_{OC} degradation.*

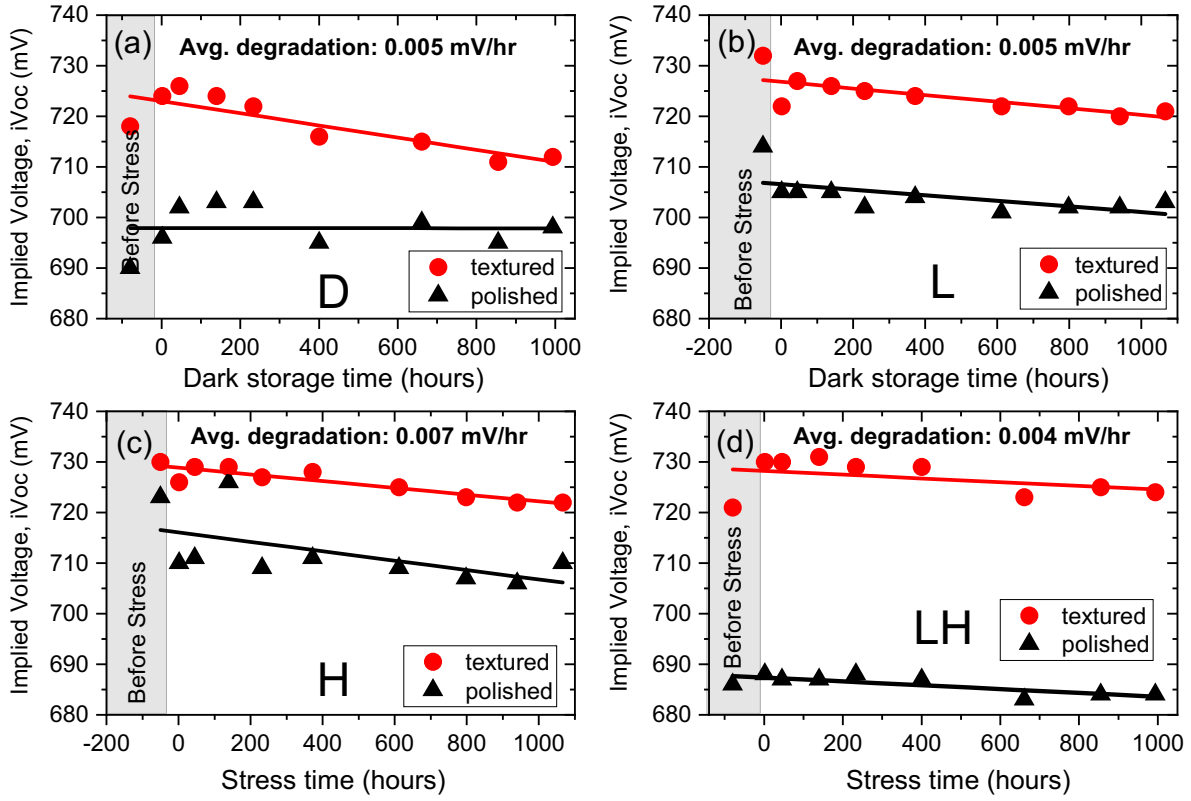

Fig. 15. iV_{OC} of symmetric (i-n)a-Si:H hetero-contact passivation as a function of 4 different stress conditions: (a) D, (b) L, (c) H and (d) LH.

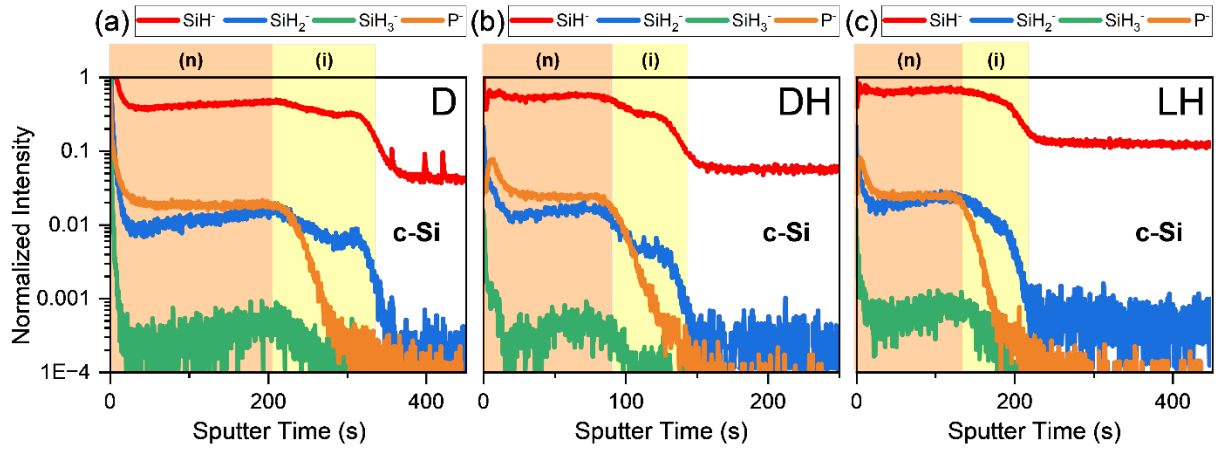

Fig. 16. ToF-SIMS depth profiles of (i-n)a-Si:H stack on Si, where (a) was taken from the sample exposed to the D condition, (b) the H condition, and (c) the LH condition. These depth profiles were taken after 1000 hours of stress exposure.

In this section, ALT results were reported and discussed for all three SHJ intermediate symmetric structures [(i)a-Si:H, (i-p)a-Si:H, and (i-n)a-Si:H]. The results from the (i)a-Si:H

layer ALT show a complex degradation mechanism masked by surface oxidation of thin (i)a-Si:H. However, we found no changes in hydrogen by ToF-SIMS depth profile. This result means that other explanations should be explored for describing the passivation degradation of (i)a-Si:H layers. We found the front (i-p)a-Si:H heterojunction stack to show a large amount of hydrogen effusion throughout the (p)a-Si:H layer under H and LH stress via ToF-SIMS. However, the iV_{OC} degradation is observed only under H stress but not with LH stress. This suggest that the presence of light perhaps anneals out defects[17,21] that are created by hydrogen loss from H stress. Additionally, the (i-n)a-Si:H BSF layers do not show the same hydrogen migration trend. These results indicate that the (i-p)a-Si:H heterojunction under H stress is the major contributor to passivation degradation of these symmetric structures, and likely also to V_{OC} loss in full SHJ cell structures, which will be discussed later in this report.

Task 2: Develop *in-situ* FTIR measurement setup capable of heating the sample to 400°C and white light illumination

Milestone 2.1: Demonstrate in-situ FTIR of a-Si:H passivated Si wafers with varying temperature (25 – 400 °C).

Milestone 2.2: Quantitative analysis of SiH, SiH_2 bonding in a-Si:H passivated Si with iV_{OC} > 740 mV under heat and light.

Summary: An existing FTIR setup (Magna 560) is modified to heat and illuminate the samples inside a high vacuum (10^{-6} Torr) chamber. The geometry of the sample manipulator is ideally suited for exposing the sample to white light illumination through a silica window, while the sample is heated by a resistive tungsten wire mounted adjacent to Si surface. *The samples are tested by cyclic heating (up to 600°C) and cooling down (40°C) without any difficulties and thus meeting Milestone 2.1 of heating the sample up to 400°C.* Several (i)a-Si:H and (i-p)a-Si:H stack passivated samples are tested by in-situ FTIR measurements at up to 600°C and 0.5-sun white light illumination. These measurements are critical to understand the hydrogen microstructural changes, kinetics and hydrogen evolution activation energies. *Loss of hydrogen from (i)a-Si:H is observed only at temperatures > 300°C, while (i-p)a-Si:H stack loses hydrogen at temperatures > 200°C with two distinct activation energies: 0.4 eV mostly for HSM, and 1.6 eV for LSM. These met the Milestone 2.2 of quantitative analysis of hydrogen microstructural changes in a-Si:H passivated c-Si.*

Establishing sample heating to > 400°C

The a-Si:H samples are mounted in a high-vacuum (HV ≈ 10^{-6} Torr) chamber with an *in-situ* FTIR instrument (Magna 560). A schematic of the experimental set-up is shown in Fig. 17.

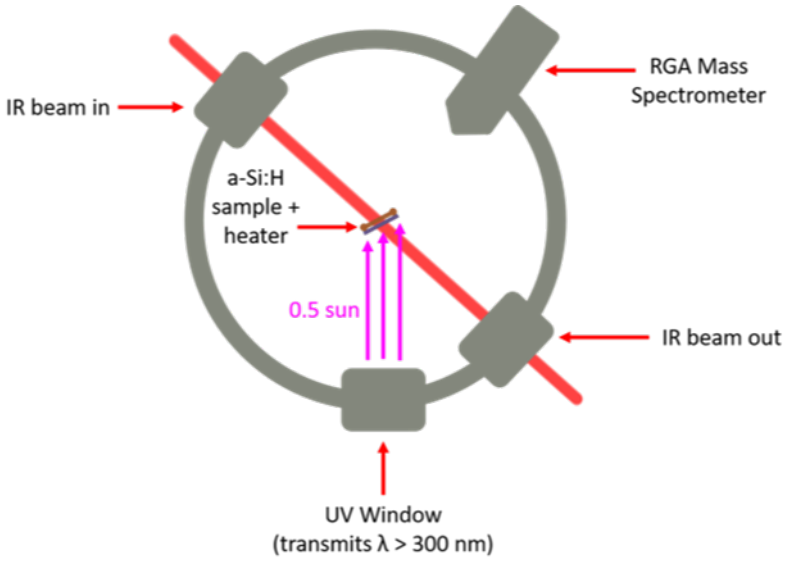

Fig. 17. Schematic setup of in-situ FTIR chamber with sample heating stage and external white light illumination source.

Symmetric (i)a-Si:H and (i-p)a-Si:H stack passivated polished c-Si samples were measured by in-situ FTIR after heating to different temperatures. The samples were first measured in as-deposited state with vacuum as a background. Each sample was then heated to the desired set temperature with heating rate approximately 2 K/s and cooled to at least 40 °C before taking the FTIR scan again. Fig. 18 (a) and (b) plot the FTIR spectra of the (i)a-Si:H heated up to 500°C, and (i-p)a-Si:H stack up to 600°C, respectively. Only a small (less than 5% by infrared intensity) reduction of SiH_X is observed up to 300°C for (i)a-Si:H [Fig. 18 (a)], but a very pronounced decrease of SiH_X is observed at temperatures > 300°C. The (i-p)a-Si:H stack, however, exhibits significant reduction of SiH_X at temperatures well below 300°C. This indicates that the hydrogen microstructures in a-Si:H in (i)a-Si:H and (i-p)a-Si:H stack are different. *This exceeds Milestone 2.1 of demonstrating in-situ FTIR measurement setup up to 400°C.*

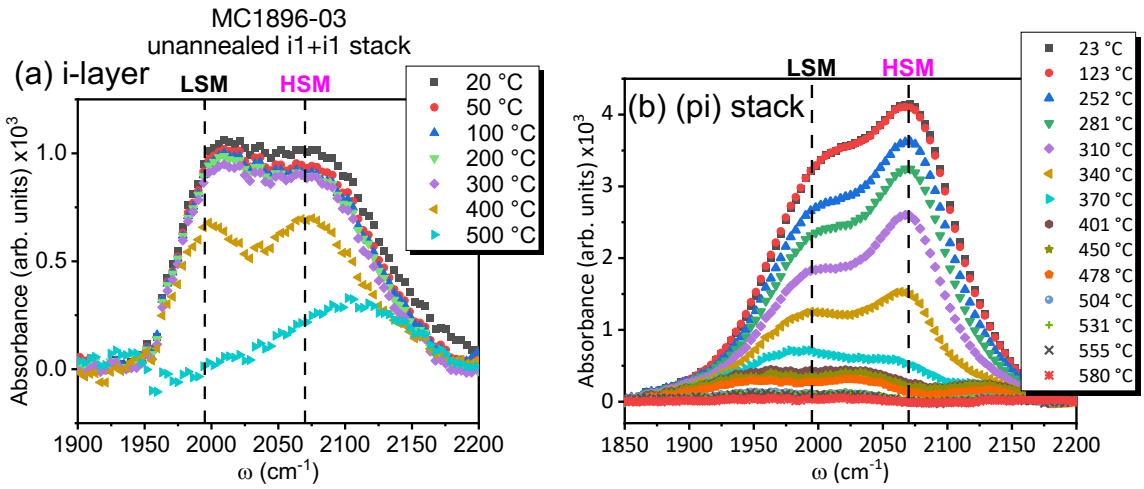

Fig. 18. In-situ FTIR for the Si–H_X stretching vibrational peak after exposing to different temperatures, (a) symmetric (i)a-Si:H and (b) symmetric (i-p)a-Si:H stack.

Quantitative analysis of SiH (LSM) and SiH_2 (HSM) bonding in a-Si:H passivated c-Si

To gain further insight, the FTIR spectra of (i-p)a-Si:H stack is deconvoluted into two Gaussian peaks labelled as HSM and LSM peaks, as shown Fig. 18 (b), which shows a decrease in HSM and LSM starting with the sample heated to 200 °C (which is same as the a-Si:H growth temperature). By 400 °C, most of the HSM was removed. Fig. 19 shows the Arrhenius plot of fractional decrease of integrated areas of HSM and LSM peaks of (i-p)a-Si:H stack. It is to be noted that the integrated areas under the LSM and HSM is proportional to their respective concentrations in the film stack. Interestingly, we observed a low activation energy of 0.4 eV for HSM and 1.6 eV for LSM. Such low activation energy (< 0.5 eV) likely suggests hydrogen migration of interstitial hydrogen, but not arising from any Si–H bond breaking, as suggested by computational calculation of different hydrogen energy barriers in a-Si:H films.[24] Moreover, the two modes representing SiH_x (HSM) and Si-H (LSM) chemical groups decrease in intensity according to different kinetics. This points to a complicated hydrogen migration/loss mechanism. *These results meet Milestones 2.2 of quantification of hydrogen microstructural changes with quantitative activation energies of hydrogen loss from the a-Si:H films.*

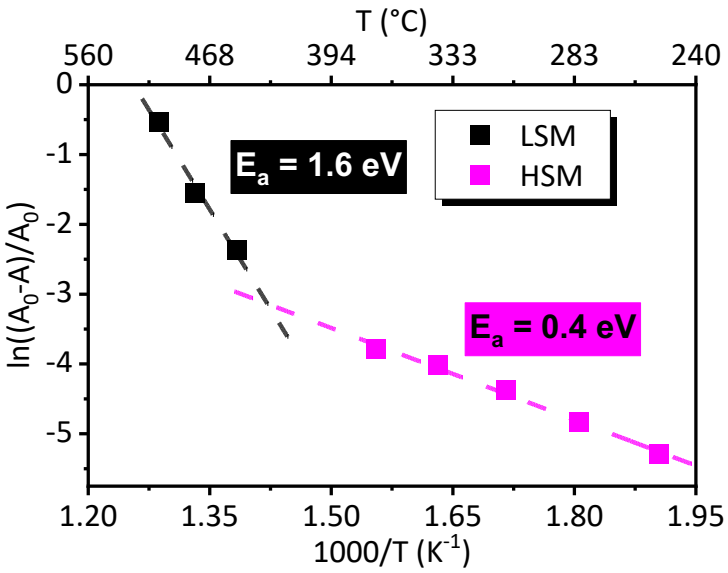

Fig. 19. Arrhenius plot of fractional loss of HSM and LSM from (i-p)a-Si:H stack passivated c-Si measured by in-situ FTIR.

In-situ FTIR with light and heat stress of (i-p)a-Si:H stack passivated Si

Several symmetrically (i-p)a-Si:H stack passivated polished c-Si samples are studied with combined heat and 0.5-sun white light illumination. The white light is generated by LED lamp. Lamp power and the dimensions of chamber and window limits the maximum intensity to 0.5-sun, as calibrated by a reference c-Si cell. The sample was constantly illuminated during heat up and cool down steps and was turned off only during spectral data collection. Fig. 20 (a) shows the FTIR spectra heated up to 300°C in conjunction with 0.5-sun illumination and (b) shows the activation energy of fractional hydrogen loss for 3 different samples. Significant hydrogen loss with activation energy of ≈0.4 eV is observed when the samples heated to > 200°C, similar to heat only FTIR experiment (Fig. 18 and Fig. 19) and ToF-SIMS depth profile of LH stressed (i-p)a-Si:H stack (Fig. 14). *This met Milestone 2.2 of quantitative hydrogen microstructural changes under light and heat.*

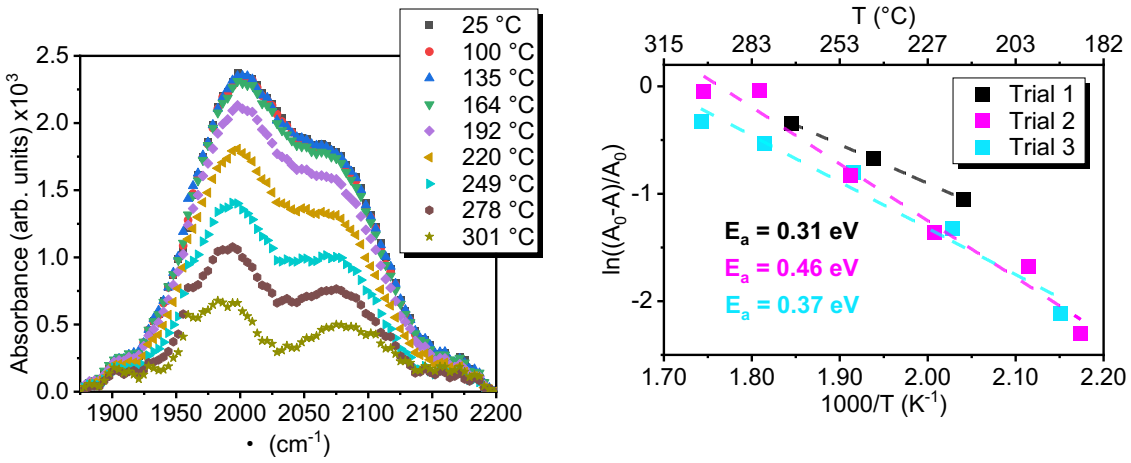

Fig. 20. (a) In-situ FTIR for the SiH_X stretching vibrational peak after exposing to combination of 0.5-sun light and temperatures, (b) Arrhenius plot of fractional loss of hydrogen from three (i-p)a-Si:H stack passivated c-Si measured by in-situ FTIR.

Task 3: SHJ cell fabrication, ALT stress exposures and ex-situ characterization of hydrogen distribution in a-Si:H and at the interfaces

Milestone 3.1: Demonstrate SHJ cell V_{OC} > 730 mV.

Milestone 3.2: Quantitative analysis of hydrogen / impurity distribution before and after stress exposures by elemental depth profiling.

Summary: The SHJ solar cells are fabricated by depositing (i-p)a-Si:H stack on one surface and (i-n)a-Si:H stack on the other surface of both textured and polished n-type Si wafers. The cell contacts are completed with both side Indium tin oxide (ITO) and Al grid in the front (i-p)a-Si:H stack and full area Al on the rear (i-n)a-Si:H stack. The highest cell V_{OC} achieved in this project is 700 mV. *This falls short by 30 mV of Milestone 3.1 of cell V_{OC} > 730 mV.* A systematic monitoring of passivation changes at each step of cell fabrication process identifies that a significant passivation loss occurs during ITO sputter deposition that causes reduction of final cell V_{OC}. This was primarily due to installation of new ITO target, which would require further process optimization to minimize/eliminate such sputter damage. SHJ cells are subjected to different stress conditions and significant V_{OC} degradation is found only for the H stress condition, similar result to the degradation of (i-p)a-Si:H heterojunction stack under H stress. ToF-SIMS depth profile of H stressed cell shows loss of hydrogen from the (p)a-Si:H layer in the region not covered by ITO, and accumulation of hydrogen at the ITO/(p)a-Si:H interface in the region covered by ITO. *This addresses the Milestone 3.2.*

SHJ cell fabrication and exposure to heat and light stresses

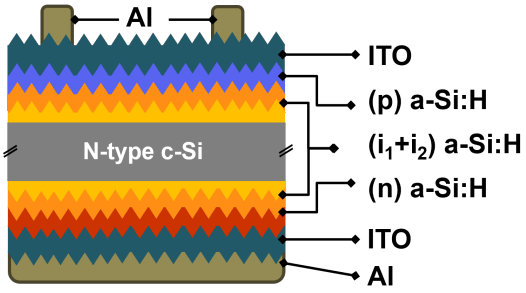

Fig. 21. Schematic of a typical SHJ cell structure fabricated in this project.

A schematic of the full SHJ cells prepared for this project is shown in Fig. 21, where the a-Si:H layers follow the same notation format used throughout this project and are deposited in a p/i/N/i/n structure. Indium tin oxide (ITO) is deposited via RF magnetron sputtering as the transparent conductive oxide for these cells, with thickness of 90 nm on each side. Ni-Al grid contacts are added to the front of the cell via e-beam deposition with thickness of 3 μm, and 0.5 μm thick Al contacts are used for the rear contact of the cell.

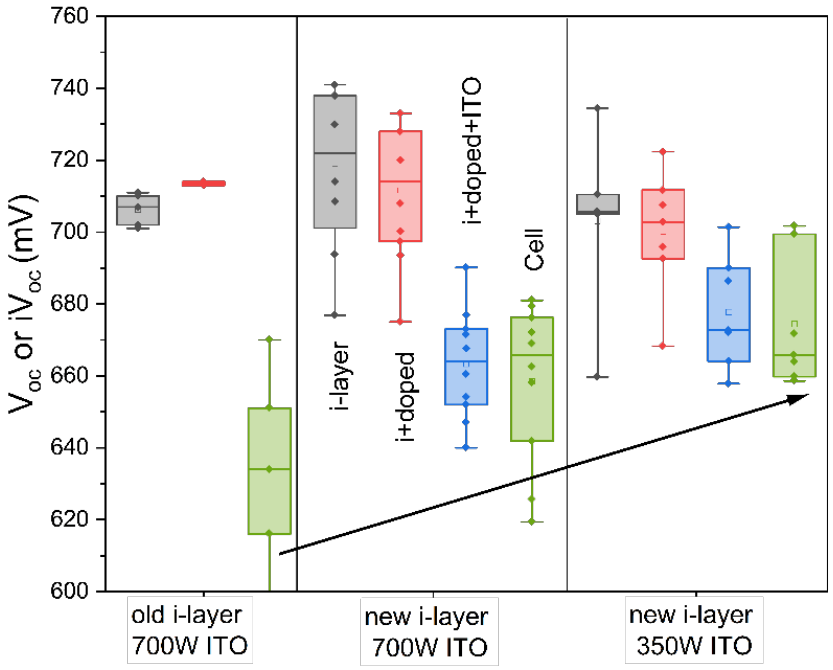

Fig. 22. Box-and-whisker plot depicting iV_{OC} data at different stages of cell fabrication process; from i-layer [*(i)a-Si:H*], i+doped layer [*(i-p)a-Si:H / (i-n)a-Si:H*], and i+doped+ITO (ITO / [*(i-p)a-Si:H / (i-n)a-Si:H* / ITO] intermediate structures. Full cell data is reported as V_{OC}.

As previously mentioned under milestone 1.2, the new (i)a-Si:H (details in Table 1) provides the best passivation, which in turn allows for the best cell V_{OC} values. Intermediate structure iV_{OC} values and final cell V_{OC} for cells made throughout this project are shown in Fig. 22. Using the "old" (i)a-Si:H condition showed a large drop after adding the ITO and contacts to the underlying amorphous structure. The use of the "new" (i)a-Si:H condition shows less loss of V_{OC} in the final cell, but was still losing 40 to 60 mV of the initial iV_{OC}. We determined that the ITO sputtering process was damaging the amorphous layers, and reduced the sputtering power from 700 W to 350 W. This lessened the loss of final V_{OC} to around 20 to 40 mV. Further optimization of the ITO sputtering process is needed to eliminate/minimize V_{OC} loss from the sputtering process. Fig. 23 shows a typical initial J-V curve of SHJ solar cells that are used for ALT stress exposures in this project.

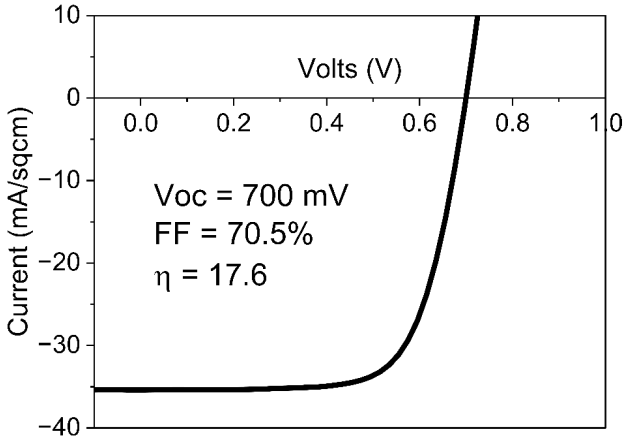

Fig. 23. Typical J-V curve for SHJ cell fabricated during this project and are used to further study under different ALT stress conditions.

ALT was performed following the same procedure and using the same stress conditions as the (i)a-Si:H and doped layer a-Si:H stack layer ALT experiments, as described in Table 2. Resulting V_{OC} values over stress time for the experiment period for each stress condition are shown in Fig. 24 (a). This experiment only shows major V_{OC} loss in the cells exposed to the H condition. The LH condition fluctuates but does not lose as much V_{OC} as the H condition. Additionally, cells made on polished versus textured wafers show only a marginal difference in V_{OC} degradation behavior for the LH condition. V_{OC} trends for L and D stress exposure are reported in Fig. 24 (b), where both trends are similar, and the V_{OC} remains stable for the entire experiment period.

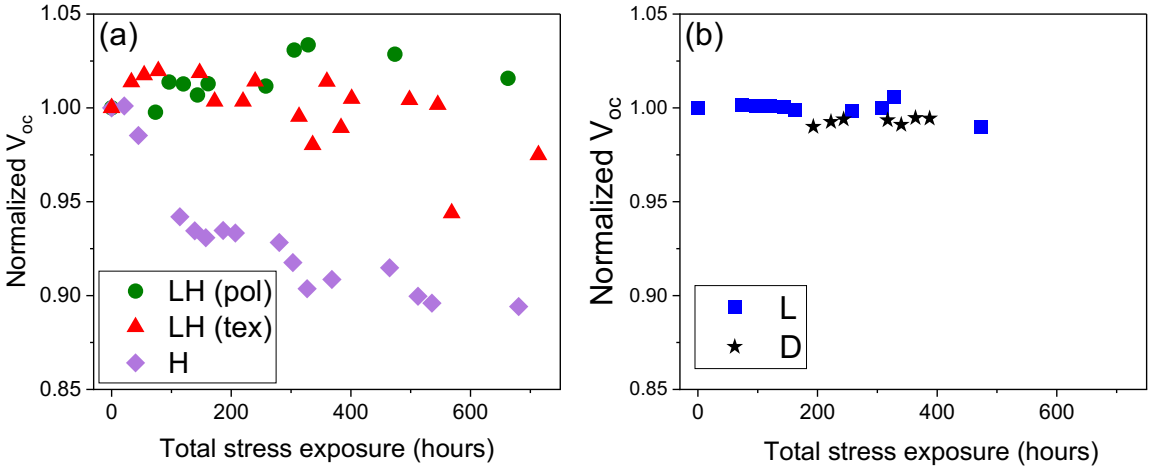

Fig. 24. Cell V_{OC} trends in full cells exposed to (a) LH (polished and textured wafers) and H stress conditions and (b) the L and D stress conditions. Unless otherwise noted, data is taken from cells made using textured wafers.

These cell degradation results are in line with the iV_{OC} trends observed from the symmetric (i-p)a-Si:H passivated structures, where the H condition shows the most iV_{OC} loss of all applied stress conditions. However, the cells exposed to LH stress do not show major V_{OC} loss, also similar to the trend observed in the (i-p)a-Si:H stack structure. *These results emphasize the conclusion from the ALT experiments performed on intermediate structures during this project: that heat is the major contributor to iV_{OC} and V_{OC} loss, and the front heterojunction consists of the (i-p)a-Si:H layers most contributing to this loss.*

The ToF-SIMS depth profile obtained from full cell through the front side of the cell (i-p)a-Si:H stack is shown in Fig. 25. Two separate regions of the cell (p)a-Si:H surface are analyzed to observe changes in hydrogen related species; the region outside of ITO deposition and the region with the ITO contact, where profiles are taken by sputtering through the entire ITO layer and (i-p)a-Si:H stack. Fig. 25 (a) shows the profile from outside the ITO area before the cell was exposed to H stress, shows the most hydrogen content in all three Si-H_x configurations. Fig. 25 (b) shows the profile taken from the same outside of the ITO area after stress and shows the most hydrogen loss in all Si-H_x configurations. Fig. 25 (c) shows the profile taken through the ITO layer, where hydrogen is shown to accumulate at the ITO/(p)a-Si:H interface from the presence of a new peak at around 350s sputtering time observed in all three Si-H_x depth profiles reported. These results point to ITO working as a capping layer, preventing hydrogen from fully leaving the amorphous layers. Additionally, these results allude to hydrogen movement being a contributing factor to the cell's V_{OC} loss (Fig. 24).

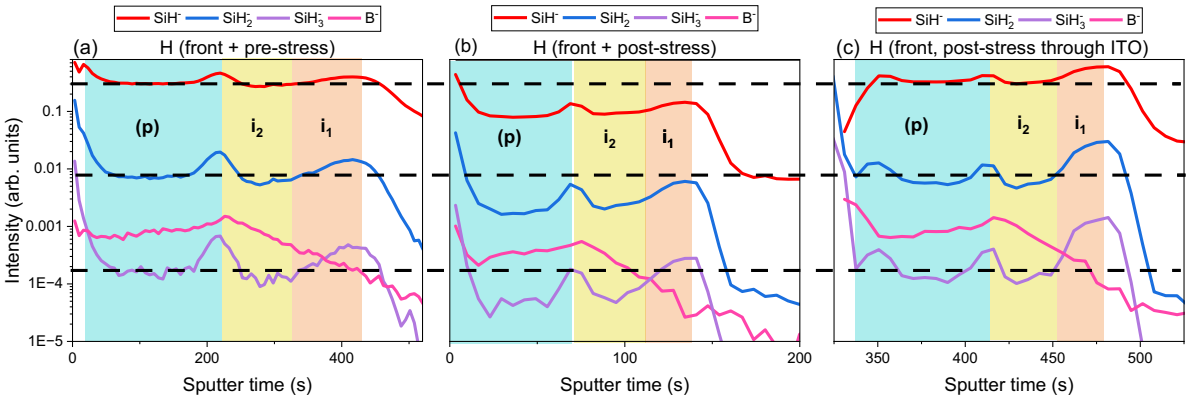

Fig. 25. ToF-SIMS depth profiles of full cells exposed to the H stress condition. These profiles were taken from (a) the front of the cell outside of ITO contact area before stress was applied, (b) the front of the cell taken outside of ITO contact area after the full stress exposure period, (c) the cell inside the cell area through the ITO layer after the full stress exposure period.

Task 4: Hydrogen migration/evolution kinetics by in-situ FTIR and comparison to the kinetics of surface passivation

Milestone 4.1: Determine activation energies of hydrogen evolution and correlate to the degradation of τ_{eff} & iV_{OC}.

Summary: The activation energies for hydrogen loss from the (i-p)a-Si:H stack by temperature-dependent in-situ FTIR have been shown and described in Task 2. In this task, similar heat induced changes in τ_{eff}, iV_{OC}, and surface recombination velocities (S) are studied by ex-situ QSSPC measurements along with the ex-situ FTIR. Both (i)a-Si:H and (i-p)a-Si:H passivated HJ stack on textured and polished Si samples are sequentially annealed at temperatures (T_{anneal}) from 100˚C to 300˚C in 25˚C steps, and iV_{OC} by QSSPC and FTIR spectra of Si–H stretching vibration are recorded after each T_{anneal}. Significant increase of S, which is proportional to interface defect density (D_{it}), is observed only for (i-p)a-Si:H stack at T_{anneal} > 200ºC with concomitant loss of SiH_X. *Activation energies for ex-situ measured* hydrogen *loss of 0.46 eV and for SRV increase of 0.60 eV are obtained, thus signifying H-loss from (i-p)a-Si:H stack is one of the primary reasons for increase in SRV and loss of V_{OC} in SHJ structure. This addresses Milestone 4.1.*

Temperature dependence and kinetics of H-microstructure and interface recombination

Both (i)a-Si:H and (i-p)a-Si:H stack passivated c-Si samples are subjected to thermal annealing for 30 mins at each varying temperatures in high vacuum (<10^{-6} Torr) to investigate changes in c-Si surface passivation and hydrogen microstructures. Fig. 26 (a) and (b) show the variation of iV_{OC} with T_{anneal} for (i)a-Si:H and (i-p)a-Si:H stacks, respectively. Both polished and textured c-Si samples exhibit similar trends of iV_{OC} variation with T_{anneal}, but textured samples change more than the polished samples, likely due to higher surface area of textured Si. However, a striking difference is that the iV_{OC}

increases slightly for i-layer [Fig. 26(a)] while it decreases substantially for the (i-p)a-Si:H stack [Fig. 26(b)], especially at T_{anneal} > 200˚C. Fig. 26 (c) and (d) show the corresponding FTIR absorbance of Si–H stretching mode on polished Si samples for both (i)a-Si:H and (i-p)a-Si:H stack after annealing at different T_{anneal}. The SiH_X peak for (i)a-Si:H does not change appreciably, while an obvious decrease of SiH_X peak intensity at T_{anneal} > 200˚C is observed for (i-p)a-Si:H stack. This indicates a direct correlation between changes in hydrogen content (proportional to the peak area) with the variation of iV_{OC} in both passivated HJ stacks.

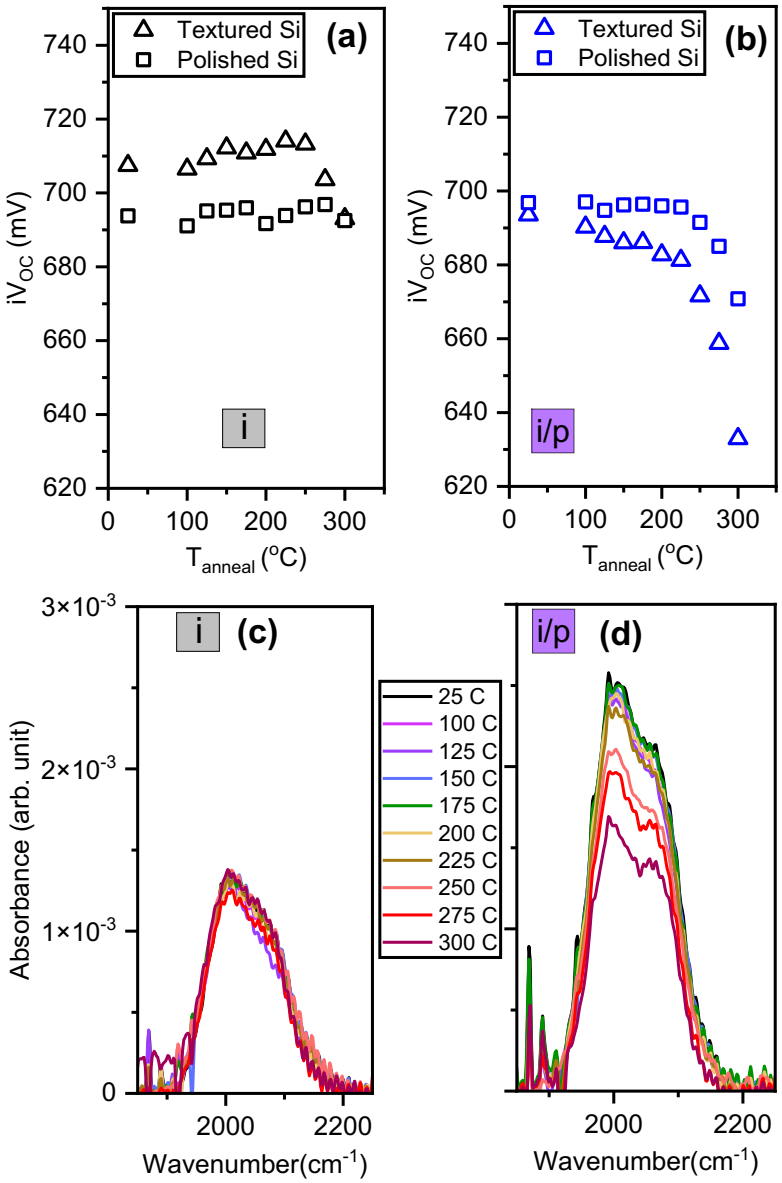

Fig. 26. Variation of iV_{OC} with T_{anneal} for polished and textured Si passivated by (a) (i)a-Si:H, and (b) (i-p)a-Si:H stack. (c) and (d) show the corresponding FTIR Si–H peak at different T_{anneal} on polished Si.

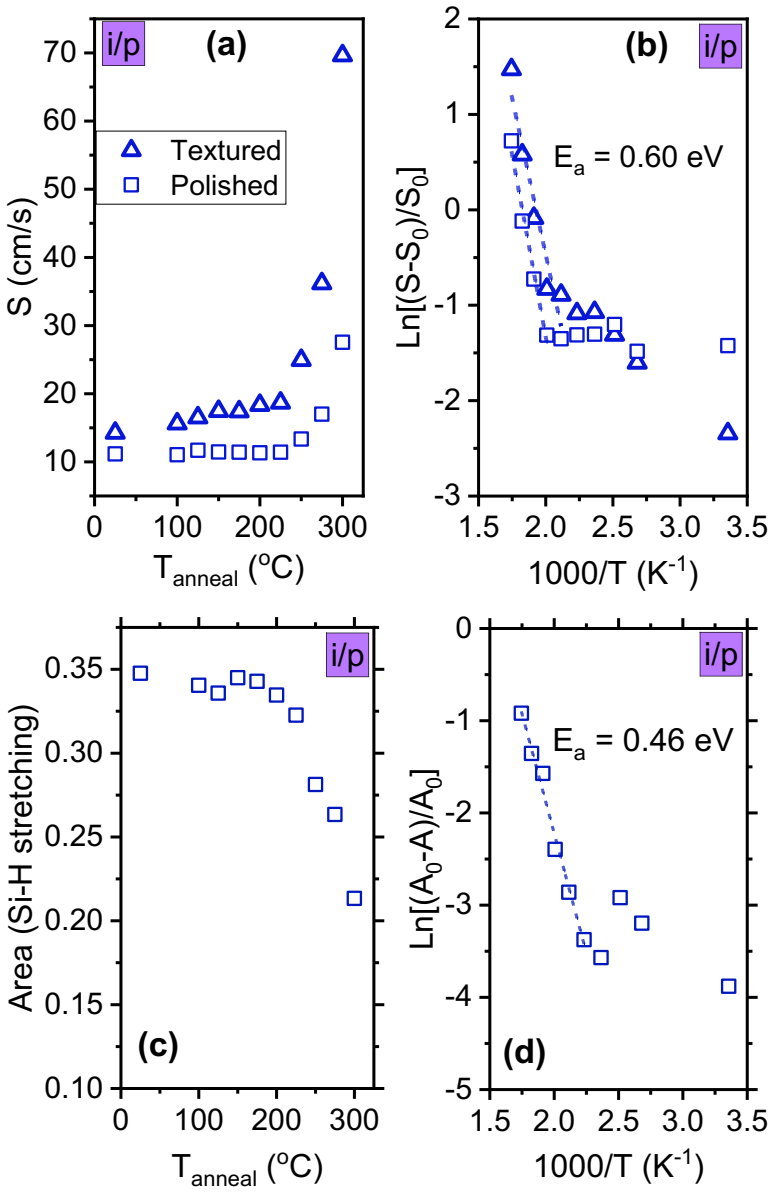

Fig. 27. (a) increase of S with T_{anneal}, (b) Arrhenius plots of fractional increase in S, (c) decrease of Si–H stretching peak area with T_{anneal}, and (d) Arrhenius plot of fractional decrease in Si–H stretching peak area (hence hydrogen-content) of (i-p)a-Si:H HJ stack.

Fig. 27 shows the T_{anneal}-dependent S, estimated from τ_{eff}, and the Si–H peak area in (a) and (c), respectively; while Arrhenius plots of fractional increase in S and decrease of Si–H peak area are shown in (b) and (d), respectively. *Activation energies of 0.6 eV for increase in S on both polished and textured samples, and 0.46 eV for loss of hydrogen from the (i-p)a-Si:H stack on polished sample suggest that the two phenomena are correlatively linked to the same process that causes loss of hydrogen and increase of recombination due to increase in D_{it}. This addresses Milestone 4.1.* Such low activation

energy (0.5 – 0.6 eV) is not sufficient for Si–H bond breakage, is likely indicative of hydrogen migration from weakly bonded Si–H (possibly analogous to interstitial hydrogen diffusion in crystalline Si) and formation of out-diffusing H_2.

8. Significant Accomplishments and Conclusions:

We undertook a challenging task of developing a novel in-situ FTIR measurement technique to identify stress conditions, layer(s), and interface(s) responsible for V_{OC} degradation in all-important record efficiency SHJ cell technologies and correlate hydrogen microstructural changes to the surface/interface passivation degradation. We met many of the milestones set forth and fell short on a couple of milestones, but several innovations and key accomplishments regarding V_{OC}-degrading pathways are identified in this work, which would provide technical directions towards mitigating performance degradation of SHJ solar cell. These include:

a) Degradation of surface passivating thin (10 nm) intrinsic a-Si:H layer by itself is minimal; complexity of studying (i)a-Si:H passivation arises due to unavoidable surface oxidation of uncapped (i)a-Si:H, which is not relevant for SHJ cell configuration with overlying protective layers.

b) V_{OC} degradation of SHJ cells occurs majorly at the (i-p)a-Si:H HJ passivation stack with associated hydrogen loss from the (p)a-Si:H layer.

c) Correlative V_{OC} degradation and hydrogen loss occurs only under dark heat stress. Combination of light and heat stress causes hydrogen loss similar to dark heat but no V_{OC} degradation, suggesting light-induced defect annealing with additional defect chemistry.

d) Activation energy of increase in SRV (defect generation) in (i-p)a-Si:H stack under H stress is ≈ 0.6 eV, while activation energy of hydrogen loss from (i-p)a-Si:H stack is ≈ 0.4 eV, indicative of presence of weakly bonded Si–H (analogous to interstitial hydrogen in crystalline Si) in SHJ a-Si:H stack.

9. Path Forward:

This project has shown an unambiguous correlative agreement between hydrogen microstructural changes and hydrogen loss with the defect creation in (i-p)a-Si:H SHJ structures under heat stress, but such correlation cannot be established with combined light and heat stress. This suggests a competing defect reduction (annealing) mechanism is in play in the presence of light. This has also been sporadically reported in literature, and requires further deeper understanding with both theoretical modeling and experimental measurements of defects. A concerted effort is required for critical understanding of both hydrogen microstructural changes along with defect and interface charge chemistries under different stress conditions to design mitigation strategies of V_{OC} degradation in SHJ solar cells. Furthermore, structural changes at the TCO/doped a-Si:H interfaces need to be deciphered to eliminate any potential contact related V_{OC} degradation. We have noticed a big effect of ITO process conditions to the V_{OC} loss in

this project, which require much more detailed investigation and optimization. This was limited due to shorter time frame of this SIPS project.

10. Products:

Publications:

1. U. K. Das, T. K. Mouri, M. Piña, T. Parke, D. R. S. Quinones, and A. V. Teplyakov, “Interface hydrogen and passivation of amorphous Silicon / crystalline Silicon heterojunction” – Proc. of the 50th IEEE PVSC conference (2023).
2. D. S. Quinones, J. R. Mason, R. Norden, and A. V. Teplyakov, “Inhibition of atomic layer deposition of TiO_2 by functionalizing silicon surface with 4-fluorophenylboronic acid”, – J. Vac. Sci. Technol. **A 42**, (2024) 032402.
3. U. K. Das, M. Zeile, M. Pina, J. R. Mason, and A. V. Teplyakov, “Correlating V_{OC} degradation with hydrogen evolution kinetics in Si heterojunction stack”, – Presented in 52nd IEEE PVSC conference (2024).
4. M. Zeile, J. R. Mason, M. Piña, T. K. Mouri, D. R. S. Quinones, T. Parke, A. V. Teplyakov, and U. K. Das, “Chemical analysis of intrinsic amorphous silicon passivation layers after accelerated lifetime testing”, – Presented in 52nd IEEE PVSC conference (2024).
5. “Heat and light induced hydrogen evolution kinetics and its correlation to Si HJ passivation degradation" (under preparation).

Conference, meeting travel:

1. Ujjwal K. Das and Tasnim K. Mouri traveled to San Juan, Puerto Rico to attend and present papers in the 50th IEEE PVSC conference (June 11 – 16, 2023).
2. Ujjwal K. Das and Andrew V. Teplyakov traveled to Washington DC to attend and present the research work in the biannual SETO program review meeting held in March 25 – 26, 2024.
3. Ujjwal K. Das and Margaret (Maggie) Zeile traveled to Seattle, WA to attend and present two papers in the 52nd IEEE PVSC conference (June 9 – 14, 2024).

11. Project Team and Roles:

Ujjwal K. Das (IEC): Supervised students for experimental design of SHJ test and cell structures, ALT stress conditions, and managed the overall project.

Andrew V. Teplyakov (CBC): Supervised students for in-situ FTIR, XPS, ToF-SIMS characterizations, and helped manage project milestones and quarterly reports.

Tasnim Kamal Mouri (IEC): ALT stress exposure of passivated (pi) and (ni) stack structures and their passivation measurements.

Margaret (Maggie) Zeile (IEC): Optimization of i-layer passivation, SHJ cell processes, ALT stress exposures, and ex-situ FTIR and passivation measurements.

Noah Jones (undergraduate URM student, IEC): Ex-situ FTIR characterization in the last quarter of the project.

Dhamelyz Rosana Silva Quinones (CBC): Preliminary ToF-SIMS measurements.

Tyler Parke (CBC): Setting up of in-situ FTIR with sample heater.

Marissa Piña (CBC): Detail study of light and heat induced in-situ FTIR measurements of i-layer and (pi) stack passivated Si samples, and ex-situ ToF-SIMS characterization.

John R. Mason (CBC): Surface characterizations by XPS and ToF-SIMS.

12. References:

[1] M. Taguchi, K. Kawamoto, S. Tsuge, T. Baba, H. Sakata, M. Morizane, K. Uchihashi, N. Nakamura, S. Kiyama, and O. Oota, "HIT^{TM} Cells – High-efficiency crystalline Si cells with novel structures," Prog. Photovolt: Res. Appl. **8** (2000) 503.

[2] M. Taguchi, "Review – Development history of high efficiency silicon heterojunction solar cell: From discovery to practical use," ECS J. Solid State Sci. Technol. **10** (2021) 025002 and references therein.

[3] H. Wu, G. Wang, H. Qiu, X. Tang, Z. Sun, F. Ye, L. Fang, and X. Xu, "27.09%-efficient silicon heterojunction solar cell technology with interdigitated back contacts", Presented at the 52nd IEEE PVSC (2024), Seattle, WA.

[4] M. Taguchi, A. Yano, S. Tohoda, K. Matsuyama, Y. Nakamura, T. Nishiwaki, K. Fujita, and E. Maruyama, "24.7% record efficiency HIT cell on thin silicon wafer", IEEE J. Photovoltaics **4** (2014) 96.

[5] T. Ishii, and A. Masuda, "Annual degradation rates of recent crystalline silicon photovoltaic modules", Prog. Photovolt: Res. Appl. **25** (2017) 953.

[6] D. C. Jordan, C. Deline, S. Johnston, S. R. Rummel, B. Sekulic, P. Hacke, S. R. Kurtz, K. O. Davis, E. J. Schneller, X. Sun, M. A. Alam, and R. A. Sinton, "Silicon heterojunction system field performance", IEEE J. Photovoltaics **8** (2018) 177.

[7] J. Karas, A. Sinha, V. S. P. Buddha, F. Li, F. Moghadam, G. Tamizhmani, S. Bowden, and A. Augusto, "Damp heat induced degradation of silicon heterojunction solar cells with Cu-plated contacts", IEEE J. Photovoltaics **10** (2020) 153.

[8] D. C. Jordan, and S. R. Kurtz, "Photovoltaic Degradation Rates - an Analytical Review: Photovoltaic Degradation Rates.", Prog. Photovolt. Res. Appl. **21** (2013) 12.

[9] F. Carigiet,C. J. Brabec, and F. P. Baumgartner, "Long-Term Power Degradation Analysis of Crystalline Silicon PV Modules Using Indoor and Outdoor Measurement Techniques", Renew. Sustain. Energy Rev. **144** (2021) 111005.

[10] R. Jones-Albertus, D. Feldman, R. Fu, K.Horowitz, and M. Woodhouse, "Technology Advances Needed for Photovoltaics to Achieve Widespread Grid Price Parity: Widespread Grid Price Parity for Photovoltaics," Prog. Photovolt. Res. Appl. **24** (2016) 1272.

[11] M. Woodhouse, R. Jones-Albertus, D. Feldman, R. Fu, K. Horowitz, D. Chung, D. Jordan, and S. Kurtz, “On the Path to SunShot. The Role of Advancements in Solar Photovoltaic Efficiency, Reliability, and Costs,” NREL/TP--6A20-65872, 1253983; 2016; p NREL/TP--6A20-65872, 1253983.

[12] S. De Wolf, B. Demaurex, A. Descoeudres, and C. Ballif, “Very fast light-induced degradation of a -Si:H/ c-Si(100) interfaces,” Phys. Rev. B, vol. **83** (2011) 233301, 2011.

[13] S. Bernardini, and M.I. Bertoni, “Insights into the degradation of amorphous silicon passivation layer for heterojunction solar cells. Phys. Status Solidi A, **216** (2018) 1800705.

[14] H. Plagwitz, B. Terheiden, and R. Brendel, “Staebler–Wronski-like formation of defects at the amorphous-silicon–crystalline silicon interface during illumination,” J. Appl. Phys. **103** (2008) 094506.

[15] R. Vasudevan, I. Poli, D. Deligiannis, M. Zeman, A. H. M. Smets, “Light-induced effects on the a-Si:H/c-Si heterointerface,” IEEE J. Photovoltaics **7** (2017) 656.

[16] S. De Wolf, and M. Kondo, “Nature of doped a-Si:H/c-Si interface recombination,” J. Appl. Phys. **105** (2009) 103707.

[17] E. Kobayashi, S. De Wolf, J. Levrat, G. Christmann, A. Descoeudres, S. Nicolay, M. Despeisse, Y. Watabe, and C. Ballif, “Light-induced performance increase of silicon heterojunction solar cells,” Appl. Phys. Lett. **109** (2016) 153503.

[18] W. Liu et al., “Light-induced activation of boron doping in hydrogenated amorphous silicon for over 25% efficiency silicon solar cells,” Nature Energy **7** (2022) 427.

[19] J. Cattin, L. L. Senaud, J. Haschke, B. Paviet-Salomon, M. Despeisse, C. Ballif, and M. Boccard, “Influence of light soaking on silicon heterojunction solar cells with various architectures,” IEEE J. Photovoltaics **11** (2021) 575.

[20] B. Wright, C. Madumelu, A. Soeriyadi, M. Wright, and B. Hallam, “Evidence of a light-induced degradation mechanism at elevated temperatures in commercial n-type silicon heterojunction solar cell,” Sol. RRL **4** (2020) 2000214.

[21] C. Madumelu, B. Wright, A. Soeriyadi, M. Wright, D. Chen, B. Hoex, and B. Hallam, “Investigation of light-induced degradation in n-type silicon heterojunction solar cells during illuminated annealing at elevated temperatures,” Sol. Energy Mater. Sol. Cells **218** (2020) 110752.

[22] S. W. Johnston, D. C. Jordan, D. B. Kern, D. J. Colvin, K. O. Davis, H. R. Moutinho, and G. F. Kroeger, “Degradation-related defect level in weathered silicon heterojunction modules characterized by deep level transient spectroscopy,” Sol. Energy Mater. Sol. Cells **262** (2023) 112527.

[23] D. Unruh, R. V. Meidenshahi, C. Hansen, S. Manzoor, M. I. Bertoni, S. M. Goodnick, and G. T. Zimanyi, “From femtoseconds to gigaseconds: The SolDeg platform for the performance degradation analysis of silicon heterojunction solar cells,” ACS Appl. Mater. Interfaces **13** (2021) 32424.

[24] A. Diggs, Z. Zhao, R. V. Meidenshahi, D. Unruh, S. Manzoor, M. Bertoni, S. M. Goodnick, and G. T. Zimanyi, “Hydrogen-induced degradation dynamics in silicon heterojunction solar cells via machine learning,” Communication Materials **4** (2023) 24.

[25] E. Centurioni, “Generalized matrix method for calculation of internal light energy flux in mixed coherent and incoherent multilayers,” Appl. Optics **44** (2005) 7532.

[26] U. J. Nsofor, L. Zhang, A. Soman, C. M. Goodwin, H. Liu, K. D. Dobson, U. K. Das, T. P. Beebe Jr., and S. Hegedus, “Analysis of silicon wafer surface preparation for heterojunction solar cells using X-ray photoelectron spectroscopy and effective minority carrier lifetime,” Sol. Energy Mater. Sol. Cells **183** (2018) 205.

[27] H. Sai, “Impact of intrinsic amorphous silicon bilayers in silicon heterojunction solar cells,” J. Appl. Phys., vol. **124** (2018) 103102.

[28] W. Liu, L. Zhang, R. Chen, F. Meng, W. Guo, J. Bao, and Z. Liu, “Underdense a-Si:H film capped by a dense film as the passivation layer of a silicon heterojunction solar cell,” J. Appl. Phys., vol. **120** (2016) 175301.

[29] A. H. M. Smets, and M. C. M. van de Sanden, “Relation of the Si–H stretching frequency to the nanostructural Si–H bulk environment,” Phys. Rev. B, vol. **76** (2007) 073202.